Univerzita Karlova v Praze
Matematicko-fyzikální fakulta

BAKALÁŘSKÁ PRÁCE

Zuzana Vidláková

Trigger v experimentu ATLAS

Fyzikální ústav AV ČR, v. v. i.

Vedoucí bakalářské práce: prom. fyz. Václav Vrba, CSc.
Studijní program: Obecná fyzika

2009

Chtěla bych poděkovat vedoucímu práce Václavu Vrbovi za uvedení do kolaborace ATLAS a problematiky fyziky vysokých energií. Dále bych chtěla vyjádřit díky Michalu Marčišovskému za nedocenitelné konzultace při řešení technických problémů analýzy dat a Lukáši Lipinskému za rady týkající se GNU/GPL softwaru.

Prohlašuji, že jsem svou bakalářskou práci napsal(a) samostatně a výhradně s použitím citovaných pramenů. Souhlasím se zapůjčováním práce a jejím zveřejňováním.

V Praze dne Zuzana Vidláková

Název práce: Trigger v experimentu ATLAS
Autor: Zuzana Vidláková
Katedra (ústav): Fyzikální ústav AV ČR, v. v. i.
Vedoucí bakalářské práce: prom. fyz. Václav Vrba, CSc.
e-mail vedoucího: vrba@fzu.cz

Abstrakt: V první části této práce jsou uvedeny základní myšlenky Standardního modelu a současné problémy fyziky vysokých energií. V další kapitole jsou popsány jednotlivé detektory Large Hadron Collideru (LHC) v laboratoři CERN, kde největší prostor je věnován detektorům ATLAS a CMS. Třetí kapitola je věnována triggeru a sběru dat z detektoru ATLAS. V poslední kapitole je popsána vlastní práce - analýza dat vybraného rozpadového kanálu $Z^0 \rightarrow \mu^+\mu^-$.

Klíčová slova: trigger experimentu ATLAS, fyzika vysokých energií, analýza dat

Title: Trigger in the ATLAS experiment
Author: Zuzana Vidláková
Department: Institute of Physics of the AS CR, v. v. i.
Supervisor: prom. fyz. Václav Vrba, CSc.
Supervisor's e-mail address: vrba@fzu.cz

Abstract: In firs section of this thesis are introduced basic facts of Standard Model and problems of contemporary high-energy physics. In the next section are described detectors of the Large Hadron Collider where the most significant part is dedicated to ATLAS and CMS detectors. Third section is dedicated to ATLAS trigger and Data Acquisition system. The last section describes basic analysis of one decay mode of Z^0 boson, $Z^0 \rightarrow \mu^+\mu^-$.

Keywords: Trigger in ATLAS experiment, high-energy physics, data analysis

Contents

1 Recent topics in particle physics

The particle physics belongs to one of the youngest parts of modern science and went through very quick evolution. SM does not explain all observed features of the universe. Particularly it does not explain origin of masses of elementary particles and has no answer concerning dark energy and dark matter. Further in the text, I will introduce just some of these contemporary problems which may be more or less solved in new era of super-colliders like LHC.

1.1 Brief introduction to the Standard Model

I will skip the early years of the quantum physics and I will jump directly to the introduction of Standard Model (SM). I will introduce the SM in present state and describe some basics of the contemporary problems connected to SM. SM is a consistent description of matter - particles, its properties and forces acting between them. The building blocks of the Standard Model are particles which can be sorted out by several criteria and three fundamental forces (the gravitation is excluded).

Table 1: Interaction fields and their mediating particles [ALD].

Interaction field	Mediating particle	spin
Strong field	8 gluons	1
Electromagnetic field	γ	1
Weak field	W^+, W^-, Z^0	1
Gravitation field	graviton (hypothetical)	2

The gauge theory implies that the Lagrangian is invariant under a certain continuous group of transformations. The SM group of symmetry is U(1)×SU(2)×SU(3).

1.2 Elementary Particles

According to their spin particles can be divided into two categories

Bosons

Bosons are particles with integral spin. They does not experience the Pauli exclusion principle and obey the Bose–Einstein statistics

$$n_i = \frac{g_i}{e^{(\epsilon_i - \mu)/kT} - 1} \tag{1}$$

which describes statistic behavior of bosons and where ϵ_i is energy of the single-particle state i, μ is the chemical potential, k is Boltzmann's constant, and T is the absolute temperature. As bosons don't obey the Pauli excluding principle, they can at very low temperatures create Bose-Einstein condensate. That means that several bosons can stay at the same energy level.

- Field Carriers

  As mentioned in the Table 1 there are four force fields. Every interaction is done through exchange of the corresponding mediating particle/ field carrier. Graviton is hypothetical particle for which existence is there still no evidence and it is not considered as a SM particle.

- Higgs boson

  Higgs boson remains the last undiscovered particle of the SM. It should be responsible for the mass of particles. It gains mass through so called Higgs mechanism of the spontaneous symmetry breaking which gives the mass to the massive gauge bosons (Z^0, W^-, W^+). This process requires existence of Higgs field which interacts with the gauge fields and has a nonzero value in its lowest energy state (so called vacuum energy state). Photons for example do not interact with the Higgs fields therefore they are massless. In summary the Higgs boson is a weakly interacting spin-zero particle that is the agent of electroweak symmetry breaking which will be explained in following chapters.

Figure 1: Forces and particles [Wi].

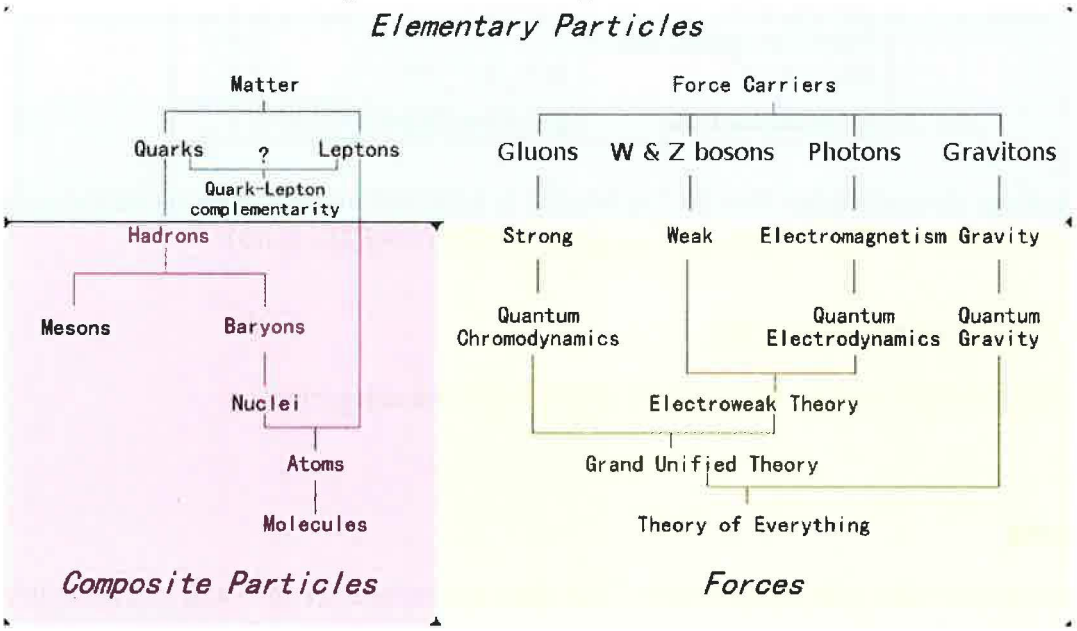

Fermions

In contrary to bosons fermions have half-integral spin. The wave function of the many-particle system of fermions is antisymmetric. Fermions obey the Fermi-Dirac distribution which describes the average number of fermions in a single-particle state i,

$$n_i = \frac{1}{e^{(\epsilon_i - \mu)/kT} + 1}, \tag{2}$$

where ϵ_i is energy of the single-particle state i, μ is the chemical potential, k is Boltzmann's constant, and T is the absolute temperature. Furthermore, Fermions can be divided into leptons and quarks.

- Leptons

  Lepton group contains electrons, muons, taus which are charged particles so they interact through electromagnetic interaction and hence through weak interaction. Neutrinos interacts only through weak interaction and this makes them objects hard to detect.

  Neutrinos are connected to several interesting phenomena. According to the SM neutrinos should be massless but solar neutrino experiments detected lower number of expected electron neutrinos from thermonuclear reactions in the solar core which can be explained by neutrino oscillations. This also implies that at least some neutrinos have certain non-zero mass. Flavour eigenstates are linear combination of mass eigenstates. They are mixed by the PNMS matrix. The probability of measuring neutrino flavour varies periodically as neutrino propagates through space. These problems are still under study and there are several ongoing experiments like KATRIN which measures electron neutrino mass or Ice cube which will measure extremely high-energy neutrinos from space and should shed light on the neutrinos oscillations.

Table 2: Leptons generations [SM].

particle	mass [Mev/c^2]	mean lifetime [s]
	Generation 1	
electron e	$m_e = 0.511$	infinite
electron neutrino ν_e	$< 2.2 \times 10^{-6}$	-
	Generation 2	
muon μ	$207 \times m_e$	2.179×10^{-6}
muon neutrino ν_μ	$<170 \times 10^{-3}$	-
	Generation 3	
tau τ	$3\,484 \times m_e$	2.9×10^{-13}
tau neutrino μ_τ	<15.5	-

- Quarks

  The attempts of describing the principles of the strong interaction led to independently postulated Quark model by M. Gell-Man and G. Zweig in 1964. Quarks unlike leptons have so called color charge. That allows them to experience the strong interaction. There are six different types of quarks/flavors: up u, down d, charm c, strange s, top t and bottom b. Their properties are summarized in table 3.

  One of the interesting facts about quarks is that they are the only particles with fractional electric charge. The idea that proton consist of two ups and one down quarks was confirmed in the 1969 at the SLAC accelerator in Stanford. The last discovered quark was

Table 3: Quarks [ALD].

Quark	spin	baryon number	charge	mass
d	1/2	1/3	- 1/3	7 MeV
u	1/2	1/3	+ 2/3	5 MeV
s	1/2	1/3	- 1/3	150 MeV
c	1/2	1/3	+ 2/3	1,4 GeV
b	1/2	1/3	- 1/3	4,3 GeV
t	1/2	1/3	+ 2/3	176 GeV

the top quark in 1995 at Fermilab. All of the properties of this quark have not yet been measured but the work is in progress (see Section 1.2). Quarks combine to form hadrons which can be subsequently divided into mesons and baryons.

Mesons are made from one quark and one antiquark and belong to bosons. Their existence was predicted by Hideki Yukawa in 1949. According to the total spin configuration there can be distinguished several meson types (for example scalar, vector, pseudovector...). All mesons are unstable. The lightest meson is the π meson [SM].

Baryons consist of three quarks and belong to fermions. Each baryon has corresponding antiparticle which has instead of quarks antiquarks. The only stable baryon is proton [SM].

1.3 Forces

In previous chapter has been mentioned that there are four fields corresponding to four fundamental forces.

- Electromagnetic force

  The electromagnetic force influences only particles with non-zero electric charge and its carrier is photon. At long distances it behaves like $1/r^2$. It has infinite range. The classical electromagnetism is represented by Maxwell equations. For formulation of the these equations it is convenient to introduce the electromagnetic antisymmetric tensor $F^{\nu\mu}$

$$F^{\mu\nu} = \begin{pmatrix} 0 & -E_x & -E_y & -E_z \\ E_x & 0 & -B_z & B_y \\ E_y & B_z & 0 & -B_x \\ E_z & -B_y & B_x & 0 \end{pmatrix} \tag{3}$$

  if we postulate that charge-four-current density

$$J^{\mu} = (\rho, \mathbf{J}) \tag{4}$$

  where ρ is an current density then continuity equation is

Figure 2: The separation of the forces [Wi]

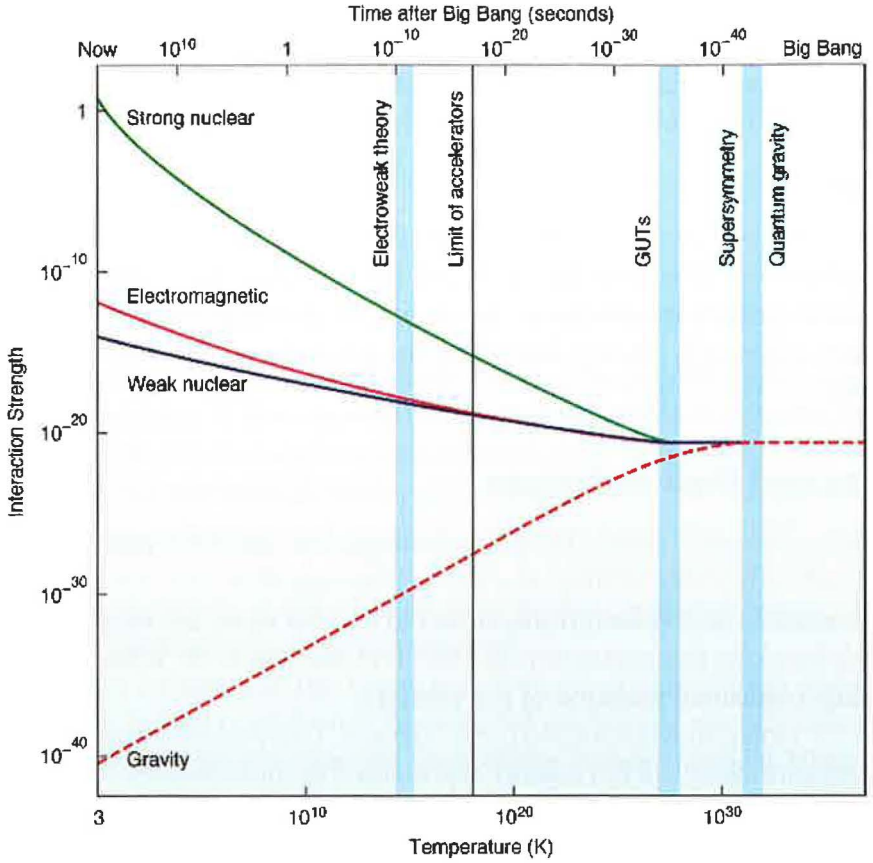

$$\partial_\mu J^\mu = 0. \tag{5}$$

The homogenous Maxwell equations correspond to

$$\partial^\lambda F^{\mu\nu} + \partial^\nu F^{\lambda\mu} + \partial^\mu F^{\nu\lambda} = 0 \tag{6}$$

where λ, μ, ν are any three of $\{0, 1, 2, 3\}$. The inhomogeneous equations take the covariant form

$$\partial_\mu F^{\mu\nu} = J^\nu. \tag{7}$$

[SM]

- Weak force

  The weak force influences only particles with non-zero flavour charge (leptons and quarks). The force carriers are Z^+, Z^- and W^0. It has finite range 10^{-18} m. Weak interaction is responsible for β decay and thermonuclear reactions. The weak interaction is the only interaction which does not conserve parity.

- Strong interaction

  The theory describing the strong interaction between quarks and gluons which have the color charge is called the Quantum Chromodynamics (QCD). The range is finite at about 10^{-15}m and the mediating particles are gluons. Quarks move within hadrons relatively freely which is result of so called asymptotic freedom.

- Gravitation

  The gravitational force is not included in the SM. It is the weakest force in the nature. At long distances it behaves like $1/r^2$ and has infinite range. The hypothetical gravitational force carriers are gravitons. According to theory gravitons must be massless and must have a spin of 2. Theory describing the gravitational force is the General Theory of Relativity.

Symmetries and their violations

The CP symmetry, where C stands for charge conjugation and P for parity, is a symmetry under which are strong and electromagnetic forces invariant if the combined CP transformation operations are made. The P violation was observed in 1956 when the weak decays of K-mesons seemed slightly breaking this symmetry. In 1957 T. D. Lee and C. N. Young realised experiment with ^{60}Co which confirmed violation of P symmetry.

In 1964 the CP violation was observed in K^0 decays. This process could answer the question why matter and antimatter are not equally represented in the universe.

Figure 3: The CP symmetry [Wi].

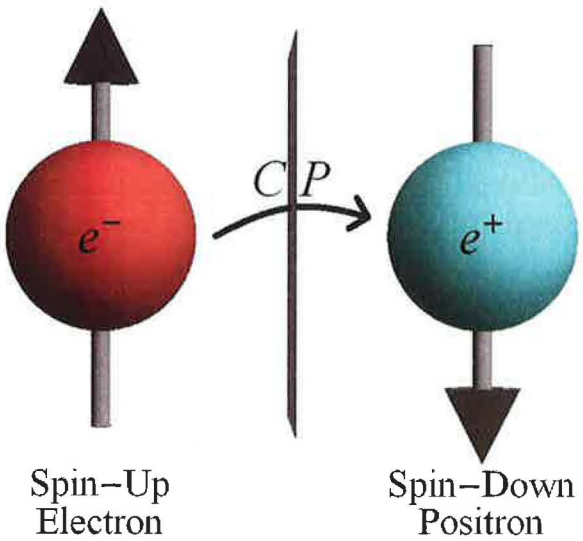

1.4 Unsolved problems

Here are some examples of problems of Standard Model:

1. The mass origin problem
2. The Theories of Unification
3. The top quark properties

The mass origin problem

It has been mentioned in section (1.2), that Higgs is one of the possible explanations of the electroweak symmetry breaking. It gives masses to the weak gauge bosons, quarks, and leptons. In 1960's the theoretical physicists started to work on unification of the weak and electromagnetic force. While building the electroweak theory it was necessary to find out the symmetry which contains both the $U(1)_{loc}$ (symmetry of the electromagnetic force) and SU(2) (symmetry of the weak force). In 1979 S. Weinberg, A. Salam and S. L. Clashow received the Nobel prize for unified electroweak interaction. Until 1983 all three bosons predicted boson - W^+, W^-, Z^0 - responsible for weak interaction had been discovered.

There are reasons to believe that the Higgs boson or other new physics should be seen on the TeV energy scale. Indirect constraints from global analyses of electroweak measurements (especially from Tevatron) suggest that the mass of the standard-model Higgs boson is less than 200 GeV. But there are several alternative mechanisms for explanation of the electroweak symmetry breaking.

The electroweak Lagrangian can be written

$$L = L_{gauge} + L_{leptons} + L_{quarks}. \tag{8}$$

where gauge Lagrangian contains four massless electroweak gauge bosons. In contrary we observe only one massless - photon. Moreover the Fermions should be according to this theory massless too [EW]. So called Higgs mechanism is process by which the bosons in any gauge theory get the non-zero mass. For hard scattering it is typical large momentum transfer and high p_T in final state qq, qg, gg scattering or annihilation. The cross section for hard scattering processes can be written [FR]

$$\sigma = \sum_{a,b} \int \hat{\sigma}_{a,b}\left(x_a, x_b\right) f_b\left(x_b, Q^2\right) f_a\left(x_a, Q^2\right) dx_a dx_b \tag{9}$$

where $\hat{\sigma}_{a,b}\left(x_a, x_b\right)$ is a hard scattering cross-section, f_i is a parton density function and x ($0 < x < 1$) is factor that effective centre-of-mass energy $\sqrt{\hat{s}}$ is smaller than the $\sqrt{s}$ of the incoming protons so $\sqrt{\hat{s}} = x\sqrt{s}$. The (9) needs higher order QCD corrections which for some processes turn out to be large (e.g. Higgs production via gg fusion). The dependency of the Higgs cross section on the center-of-mass energy are illustrated in the Figure 21. A dependency of the branching ration on the Higgs cross section can be seen in Figure 6.

Search for the Higgs

Four main processe which result in Higgs boson are shown in figure 4. The first constrains of the Higgs mass came from LEP (Large Electron-Positron) collider and then better ones from Tevatron (see figure 7). For masses below 130 GeV/c^2 are dominant Higgs to $b\bar{b}$ or to $\tau\tau$ decay modes. The $\gamma\gamma$ decay of Higgs is the most important for its mass 150 Gev/c^2. This channel is very good for LHC because all particles energy will be deposited in the calorimeters. For larger masses are relevant $H \rightarrow WW/WW^*$ and $H \rightarrow ZZ/ZZ^*$. Tevatron have better sensitivity for high-mass Higgs between 160 - 170 GeV/c^2.

Figure 4: Higgs production [FR].

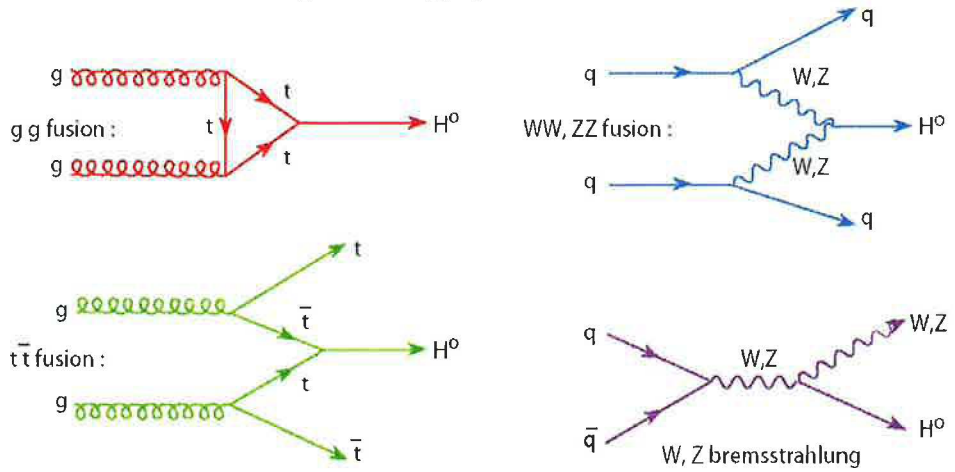

1. **Gluon fusion**
   The first channel (see figure 4) is called gluon-gluon fusion and the decay will be dominant for $m_H > 135$ GeV where $H \rightarrow WW^*/WW \rightarrow l^+l^-\nu\nu$. The $H \rightarrow ZZ/ZZ^* \rightarrow llll$ is dominant channel for higher masses of Higgs boson. The sign of this decay would be detection of opposite di-lepton and missing E_T from neutrinos. Signal contribution will be also from production of WH or ZH and qqH production. So producing the opposite dilepton source like ee, $\mu\mu$, and $e\mu$. Hence the expected spin of the Higgs boson is zero, there is possibility to use spin correlations [FR].

2. **Vector boson fusion**
   The signature of the vector-boson fusion (see figure 4) would be two high p_T forward jets and little jet activity in the central region. The best Higgs decay is $qqH \rightarrow \tau\tau$. There is a background from $Z \rightarrow \tau\tau$ but it can be reduced. Other possibility is $qqH \rightarrow W^*W \rightarrow qql^+l^-\nu\nu$. This channel is dominant for high masses where WW^*/WW and ZZ^*/ZZ are almost entirely the only decay modes of the Higgs. Main background comes here from tt production [FR].

3. **Associative production with W/Z (or W/Z bremsstrahlung)**
   Higgs boson in this case may subsequently decay in three ways $WH \rightarrow lbb\nu$ (the largest

production cross section vs. background), $ZH \rightarrow llbb$ (the smallest Higgs signal vs. less background) and $ZH \rightarrow \nu\nu bb$ (three times stronger signal vs. large background which is difficult to handle). To improve staistics one can combine analysis of all three channels together[FR].

4. **Associative production of top pair**
The final state of this decay mode will be $H \rightarrow b\bar{b}$ and two quark pairs $t\bar{t}$. There are three possible combinations of $t\bar{t}$ decays $t\bar{t} \rightarrow bjjbl\nu/bl\nu bl\nu/bjjbjj$. This channel seemed to be the best channel for LHC but the background is too high because there are several more processes which produce $t\bar{t}$ quark pairs. It is now the most promising channel at Tevatron [FR].

Figure 5: Dependency of the $\sigma\ (pp \rightarrow H + X)$ on Higgs mass for LHC

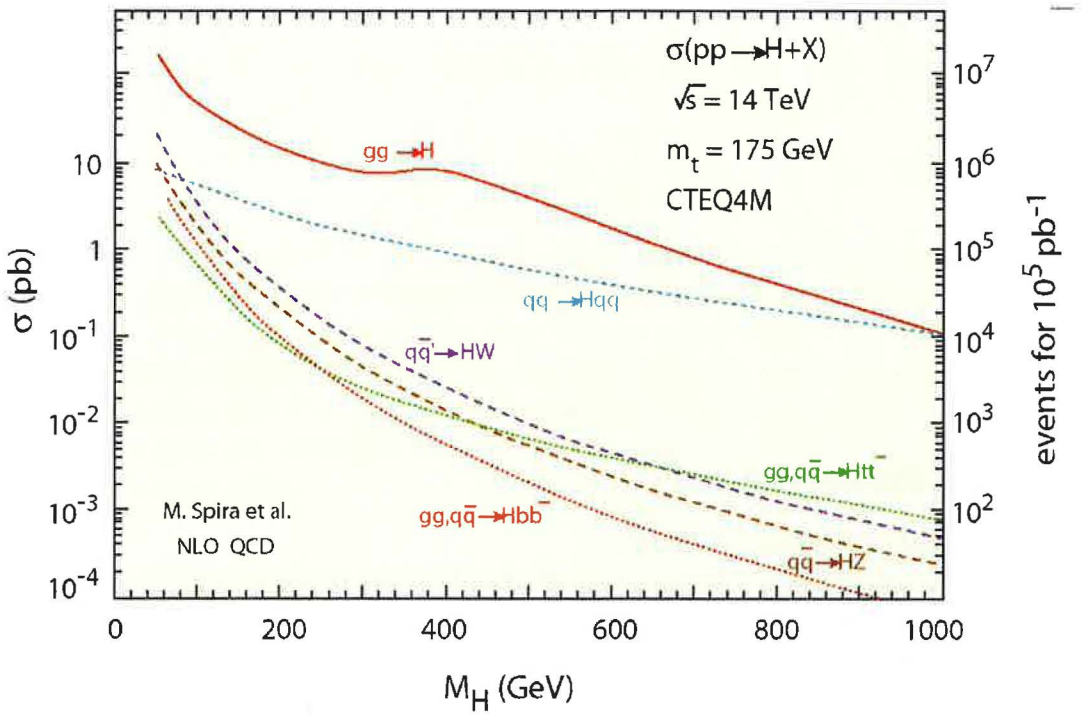

At present time (May 2009) the Higgs boson is under concentrated search of both Tevatron experiments (DØ, CDF). The result is still negative but it provides important constrans of the Higgs mass. The next improvement will bring start up of LHC in the late of 2009.

Figure 6: Dependency of the Branching ratio on the Higgs mass.

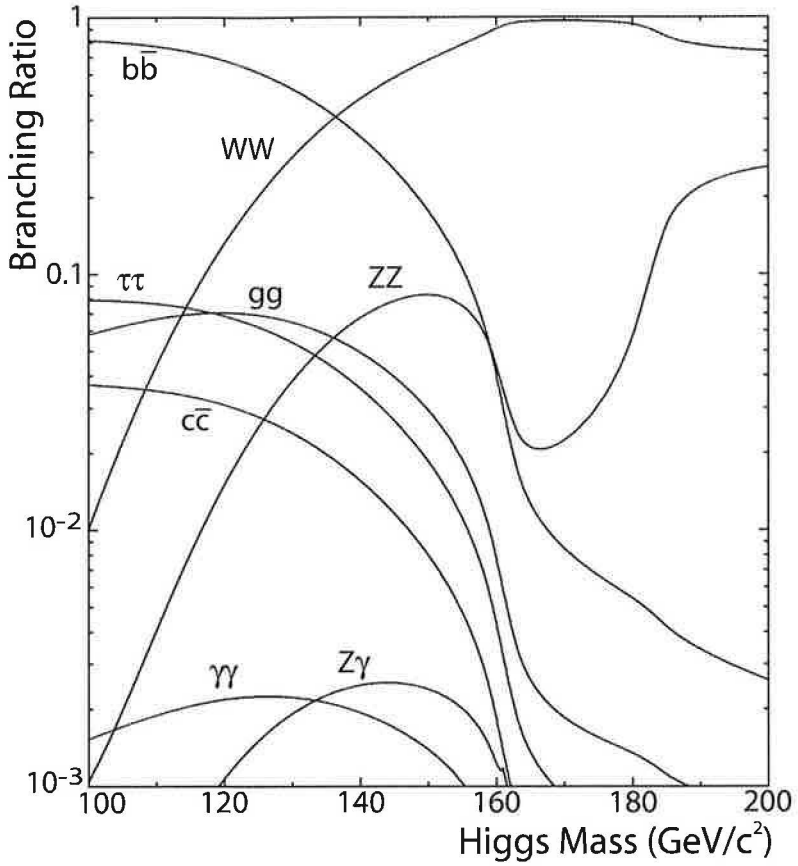

Theories of Unification

- Grand Unification Theory (GUT)
  The next logical step is to attempt to unify the electroweak theory with strong interaction. It demands to find the symmetry which consist of $U(1)_{loc} \otimes SU(2) \otimes SU(3)$. As always there are more possibilities. One of the most elegant theory which predicts existence of other mediating particles which would cause conversion between quarks and leptons. The other side of this process is that it would make proton unstable but with extremely long mean life. The strong and weak interactions will seem unified at energy level 10^{14} GeV. It is important to stress that there are many theories describing this unification process using different tools to achieve this goal.

- Supersymmetry (SUSY)
  The other possibility is Supersymmetry theory which predicts that for every boson exist a corresponding supersymmetric partner/supperpartner which spin differs of 1/2 which means that for every boson exist corresponding fermion and for every fermion corresponding boson (see table 4). Superparticles are expected to be very heavy (100-1000 $\times$ m_p) so the high energy for their production would be needed. SUSY also provides a can-

Figure 7: Combined DØ and CDF Upper Limits on SM Higgs-Boson Production [Gr2].

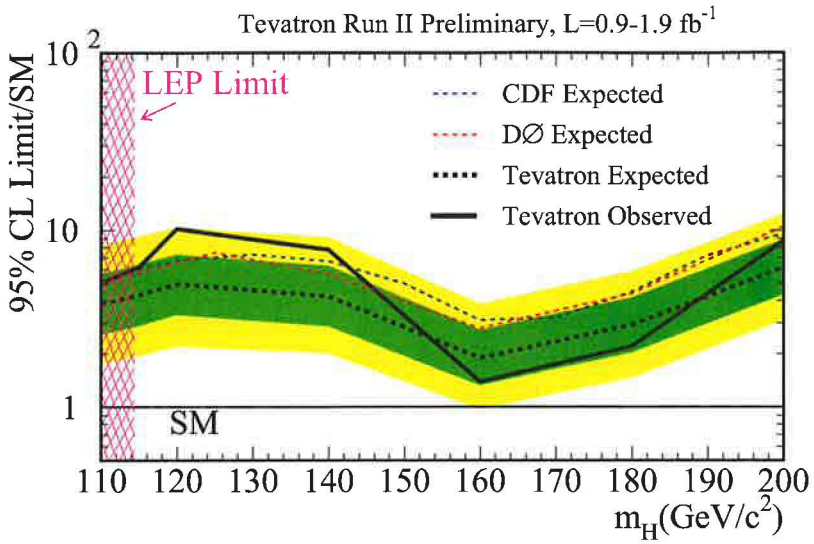

didate for explanation of the dark matter origin. The unification of all three forces at high energies (see figure 2) can be achiever in Minimal Supersymmetry Model (MSSM) within a percent-level accuracy. In MSSM, they become equal within a percent-level accuracy. On the other hand SUSY has introduced questions like: Is spacetime supersymmetry realized in nature and if so, what is the mechanism of supersymmetry breaking? LHC will easily recognise any deviation from SM on the other hand it will be difficult to find out what is its exact cause.

Table 4: Examples of particles and their superpartners [FR].

Boson	spin	Superpartner	spin	Fermion	spin	Superpartner	spin
Photon γ	1	Photino	1/2	Electron e^-	1/2	Selectron	0
Gluon	1	Gluino	1/2	Muon μ	1/2	Smuon	0
$W^{\pm}$	1	Wino$^{\pm}$	1/2	Tau τ	1/2	Stau	0
Z^0	1	Zino^0	1/2	Neutrino ν	1/2	Sneutrino	0
Higgs H	0	Higgsino	1/2	Quark	1/2	Squark	0

Top Quark

Top quark may serve as a window to new physics beyond the SM. Top was discovered in 1995 at Tevatron. Most of the properties of this quark have not yet been experimentally measured at all and even the basic ones with not high precission (mass, spin, charge, decay properties - rare

decays, gauge couplings, Yukawa coupling). The interesting facts is that top does not have any bound state which means that there can't be found any "toponium" states [FR]. Top quark has very short lifetime $\sim 10^{-24}$ s and decays before it hadronizes. The other interesting fact is that there is a SM relation between masses of W boson (m_W = 80.399 $\pm$ 0.025), Higgs boson (m_H = ?) and top quark (m_{top} = 170.9 $\pm$ 1.8 GeV/c^2 [FR])

$$m_W = \sqrt{\left(\frac{\pi \alpha_{EM}}{\sqrt{2} G_F}\right)} \frac{1}{\sin\theta_W \sqrt{1 - \triangle r}}, \tag{10}$$

where α_{EM} stands for electromagnetic constant, G_F Fermi constant, $\sin\theta_W$ is weak mixing angle (all of these constants are well-known) and $\triangle r$ radiative correction which depends on $\log(m_H)$ and m^2_{top}. If we know the masses of the top and W boson we can constrain the Higgs boson mass (see figure 8). It could also provide the test of SM because the direct Higgs mass measurement we can compare with the predictions from the radiative corrections [FR].

Figure 8: Masses of top quark and W boson and their impact on the Higgs boson mass [Gr1].

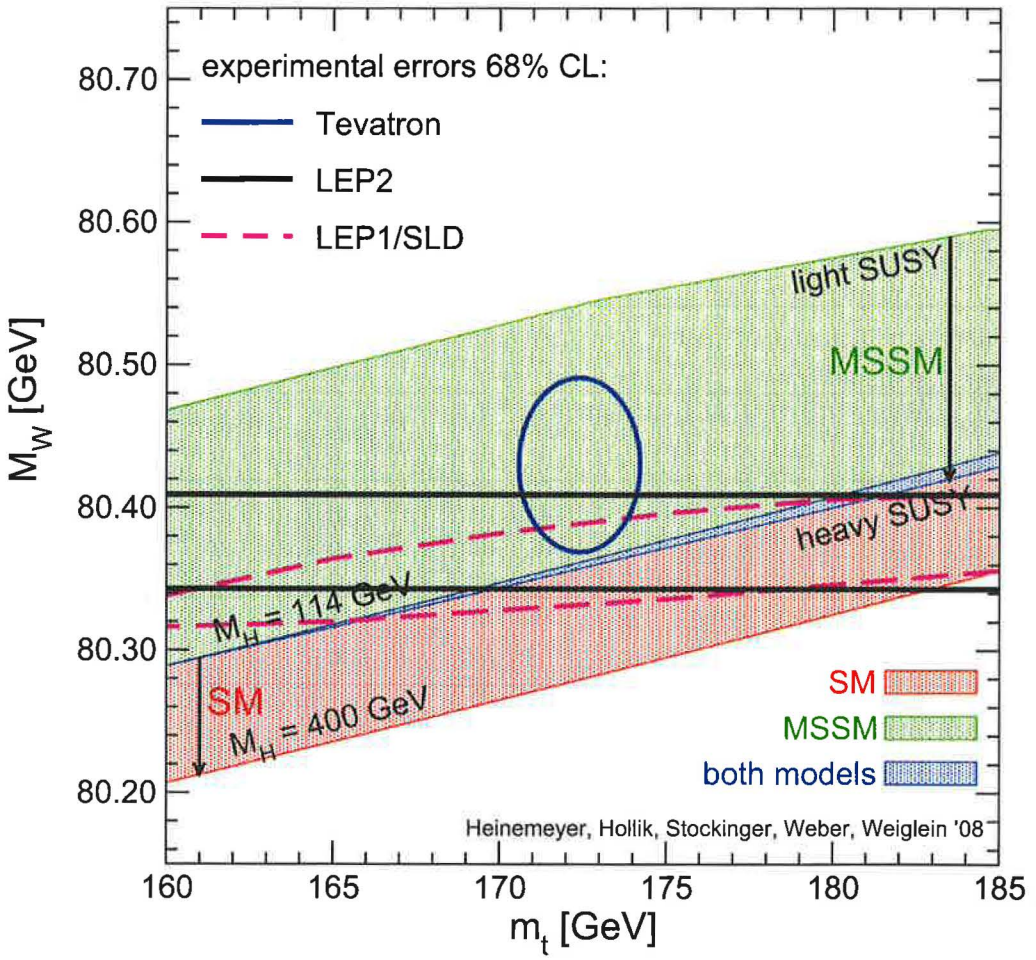

2 Overview of LHC experiments

The Standard Model has been so far tested and with the high accuracy. The theory is well corresponding to experiment up to some scale of TeV. The motivation for the Large Hadron Collider (LHC) is to scrutinize the nature of electroweak symmetry breaking for which the Higgs mechanism is presumed to be responsible (see section 1). Hence the mathematical consistency of the SM at energy scales above $\sim$ 1 TeV needs to be experimentally proved by studying of the Higgs mechanisms. The other theories such as supersymmetry, strongly-broken electroweak symmetry or technicolour can be confirmed or disproved with the help of the LHC. As in xperiment the potential of finding some other yet unknown mechanisms is always present. Furthermore, there are high hopes for discoveries that could point a way toward a unified theory or the dark matter origin. There are many more reasons for investigation of the TeV energy scale like possible discovery of the extra dimensions or demand on modification of gravity. The LHC is very well suited to the task of exploring new energy domains. The region of 1 TeV center-of-mass energy can be explored if the energy of the beam and the beam luminosity are high enough. LHC represents a seven-fold increase in energy and a hundred-fold increase in integrated luminosity with respect to Tevatron. To explore fully available potential of accelerator adequate detection systems shall be build.

The important parameter of every accelerator is luminosity $\mathcal{L}$ which is defined as

$$N_{event} = \mathcal{L}\sigma_{event}, \tag{11}$$

where N_{event} represents the event rate (number of interactions) and σ is the total cross-section of the collision. The depends on the type of interactions so $N_{event} = N_{el} + N_{inel}$ could be for elastic and inelastic (or other types) of scattering. In the real experiment step in (11) for example the detector acceptance or reconstruction efficiency which can be described by function ϵ

$$N_{event} = \mathcal{L}\sigma_{event}\epsilon. \tag{12}$$

The luminosity of the LHC will be in fully operative mode $10^{34}cm^{-2}s^{-1}$. Each proton beam will consist of 2808 bunches and each bunch will contain $1.15{\times}10^{11}$ protons per bunch. Every bunch will be separated by interval of 25 ns which means that the crossing rate will be 40 MHz. In particle physics the cross-section express the effective area for collision. The total cross-section σ_{tot} is the sum of the cross-sections due to elastic, inelastic or for other types (i.e. diffractive) of scattering which is summed.

$$\sigma_{tot} = \sum_{n} \sigma_n. \tag{13}$$

where σ_n is the integral/differential cross-section we can get after integration the cross-section over all angular yield

$$\sigma_n = \int_0^{2\pi} \int_0^{\pi} \frac{d\sigma_n}{d\Omega} sin\theta d\theta d\phi. \tag{14}$$

[CRO]

Using the optical theorem the total cross-section for pp and $p\bar{p}$ collision can be written

$$\mathcal{L}\sigma_{tot}^2 = \frac{16\pi}{1+\rho^2}\frac{dN_{el}}{dt}\bigg|_{t=0} \tag{15}$$

where $dN_{el}/dt|_{t=0}$ is an nuclear part of the elastic cross-section for t=0 and the ρ parameter has to be taken from external knowledge unless it can be measured from elastic scattering in the interference region between nuclear and Coulomb scattering. Using the previous equation for luminosity shows that luminosity L total cross-section σ can be measured independently [TOT].

$$\sigma_{tot} = \frac{16\pi}{1+\rho^2}\frac{dN_{el}/dt|_{t=0}}{N_{el}+N_{inel}}, \tag{16}$$

$$\mathcal{L} = \frac{1+\rho^2}{16\pi}\frac{(N_{el}+N_{inel})^2}{dN_{el}/dt|_{t=0}}. \tag{17}$$

There are several variables which describe important parameterisation of the measured properties. One of them is pseudorapidity η

$$\eta = -\ln\left[\tan\left(\frac{\phi}{2}\right)\right]. \tag{18}$$

where ϕ is an angle between the beam axis and the particle momentum. The transverse momentum is defined as

$$p_T = p \cdot \sin\theta \tag{19}$$

in the plane perpendicular to the beam. Most most inelastic low-p_T ($<p_T> \sim 500$ MeV) interactions are due to interactions at large distance between incoming protons which cause small momentum transfer. It means that particles in the final state have large longitudinal, but small transverse momentum. These events are called minimum bias events and will be one of the first things measured at the LHC [FR].

To find and explore the expected processes at the LHC we need proper detectors which have to satisfy several basic demands:

1. **Ability to measure precisely the missing transverse energy E_T^{miss}.**

   To measure E_T^{miss} precisely the understanding of the processes taken in the calorimeters and knowledge of the response of the calorimeter is crucial.

2. **Good b-tagging and τ identification.**
   τ is one of the indicators of the Higgs boson decay and without good b-tagging the discovery might not be possible at all.

3. **The good measurement of the high-p_T photons and leptons.**
   For measuring the produced electrons a good tracking system and electromagnetic calorimetry is needed.

4. **Good muons identification and precise measurement of their momenta**
   Leptons and expecially muons are important end-state particles for many interesting processes.

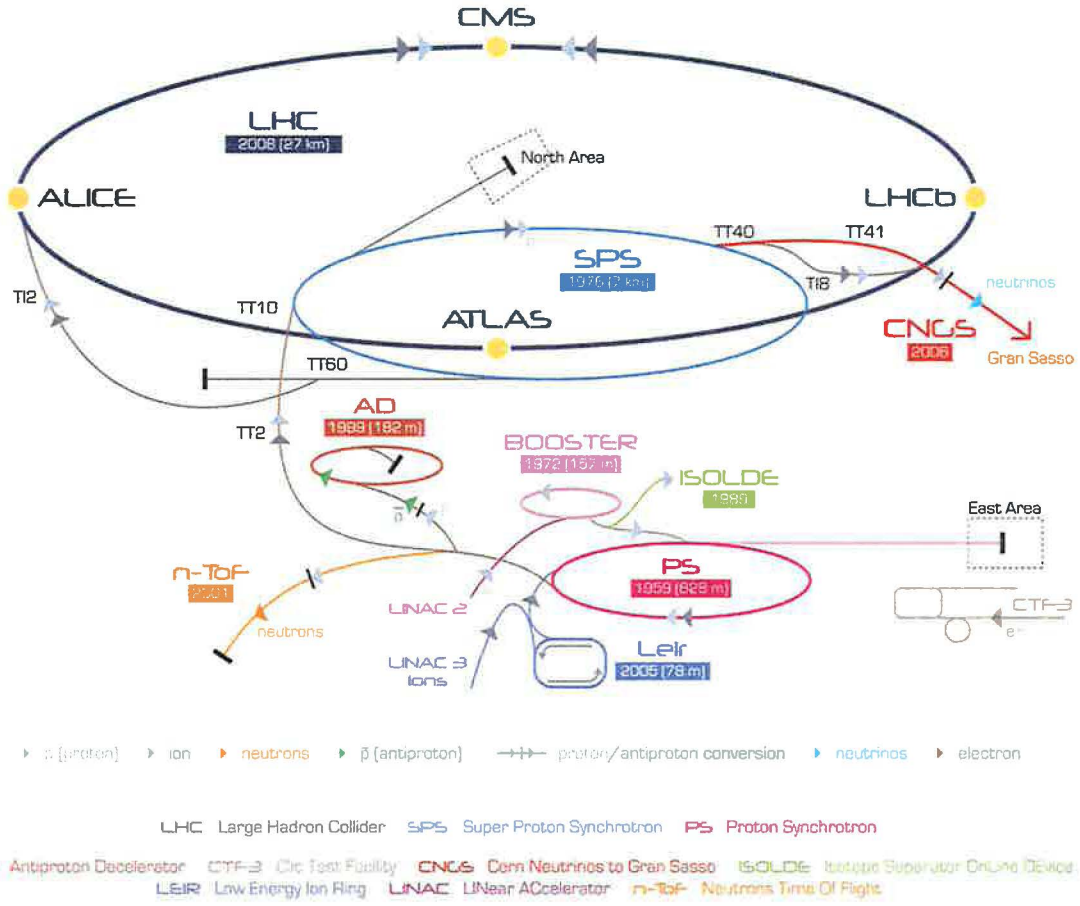
CMS
LHC
2008 (27 km)
North Area
ALICE
LHCb
TT40
TT41
SPS
1976 (2 km)
TI8
neutrinos
TI2
TT10
ATLAS
CNGS
2006
Gran Sasso
TT60
AD
1989 (182 m)
TT2
BOOSTER
1972 (157 m)
ISOLDE
1992
East Area
n-ToF
2001
PS
1959 (628 m)
CTF3
LINAC 2
neutrons
LINAC 3
Ions
Leir
2005 (78 m)
p (proton)
ion
neutrons
p̄ (antiproton)
proton/antiproton conversion
neutrinos
electron
LHC Large Hadron Collider
SPS Super Proton Synchrotron
PS Proton Synchrotron
AD Antiproton Decelerator
CTF3 Clic Test Facility
CNGS Cern Neutrinos to Gran Sasso
ISOLDE Isotope Separator OnLine DEvice
LEIR Low Energy Ion Ring
LINAC LINear ACcelerator
n-ToF Neutrons Time Of Flight

2.1 ATLAS experiment

ATLAS (A Toroidal LHC ApparatuS) is very complex detector which will in general provide measuring of particle position, momentum, mass, energy, charge, spin etc. LHC will produce protons accelerated to energies which were never reached in other experiments in the history of high-energy physic and with extremely high-rate bunch crossing made ATLAS new challenge for physicists and engineers. New unexpected phenomena can occur at high energies and ATLAS should be ready for this.

Atlas subdetectors

See figure 9 for scheme of ATLAS subdetectors.

ATLAS Inner detector

ATLAS Inner detector is situated in the Central Solenoid which provides a nominal field of 2T and allows precise measurement of charged particle trajectories. It has to operate in environment of numerous tracks, strong magnetic field and high radiation area. The outer radius of the Inner Detector is 1.15 m and the total length 7 m. The inner detector consists of three sub-detectors:

Figure 10: ATLAS Inner detector [Gr3]

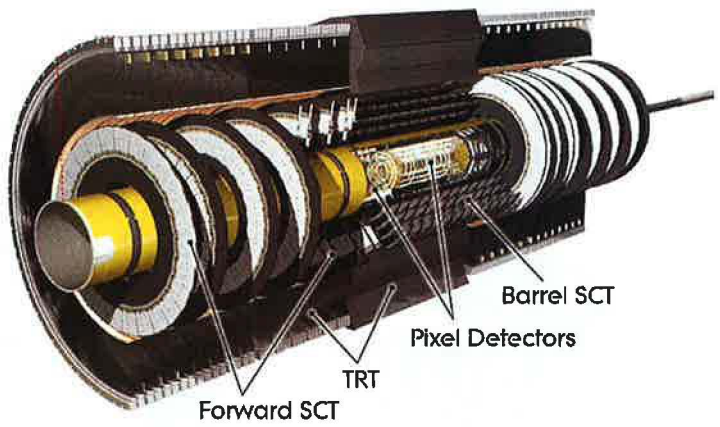

The Pixel Detector main goals are three-dimensional-vertexing, track reconstruction and secondary vertexes reconstruction for b-quark or b-jet tagging. The detector provides charged-particle tracking with high efficiency over the pseudorapidity $|\eta| < 2.5$. It consists of three

Figure 9: ATLAS detector [Gr3].

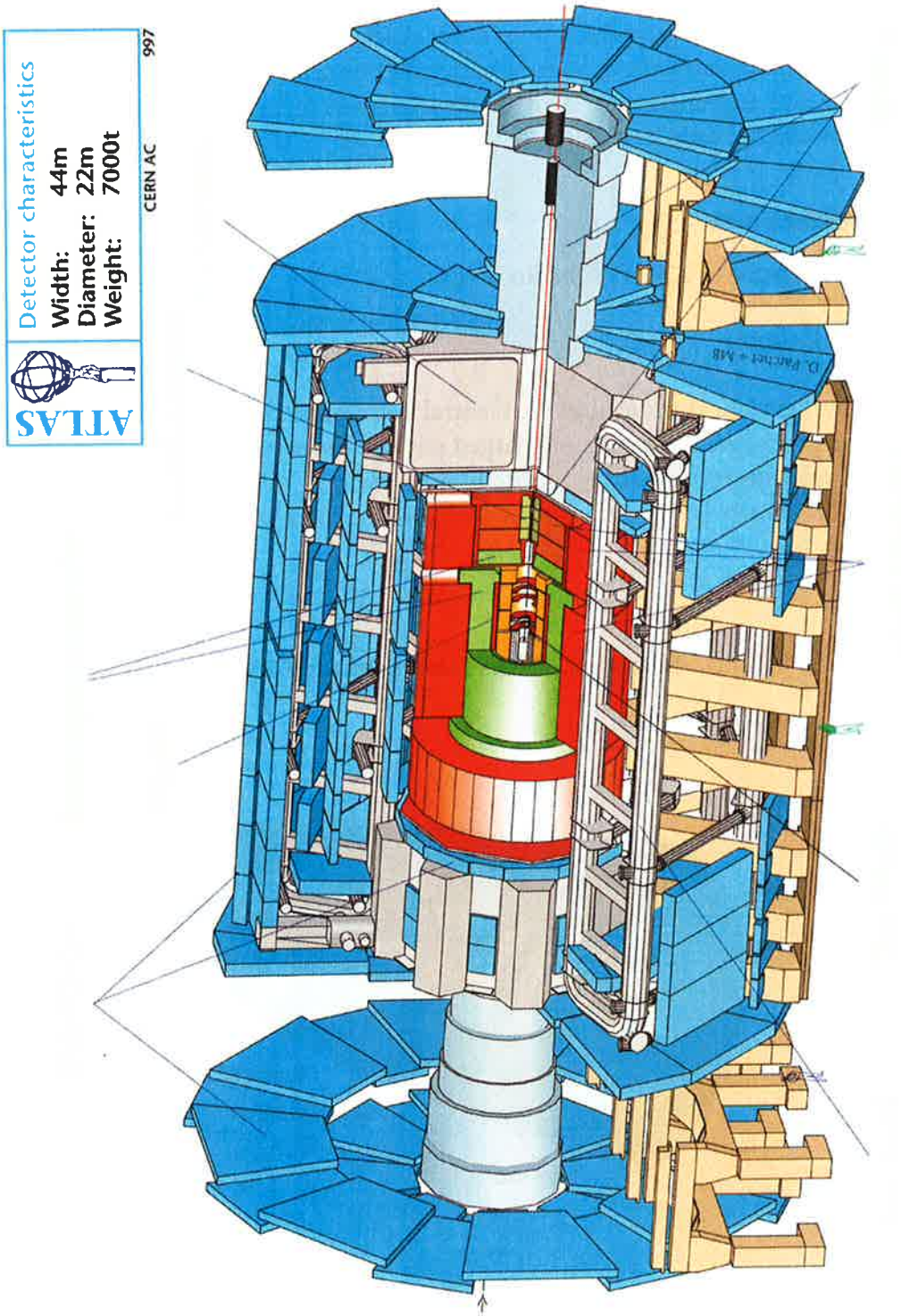

Figure 11: ATLAS Barrel Inner Detector reconstruction of $H \rightarrow b\bar{b}$ [Wi].

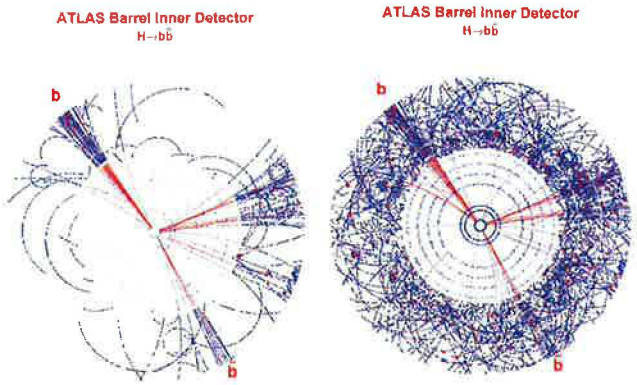

barrel layers (B-layer, Layer 1 and Layer 2) and three disks at the end of the barrels. The pixel detector is a set of pixel sensors, front-end electronics and flex-hybrids with control circuits [Pix]. One pixel sensor is a silicon wafer with size 16.4 mm $\times$ 60.8 mm. One wafer contains 46,080 pixels [Pix]. Every pixel has 50 μm $\times$ 400 μm [Pix]. This size is the smallest achievable because of the limitations of the contemporary electronics design. The pixel is able to measure the deposited energy which particle left in the detector. The total number of read-out channels is $\sim$80 million. The detector must have minimum material because of scattering and secondary interactions of the traversing particles. The materials must be very radiation hard as it has to operate without problems after a total dose of $\sim$ 500 kGy.

The SemiConductor Tracker (SCT) consist of the silicon microstrips sensors and provides the accurate measurement of tracks and momentum of the charged particles. The precision in measuring particle trajectory is 20 μm. SCT can be broken down into four concentric barrels which are located 25 $-$ 55 cm from the beams. Nine endcaps are situated at each side of the barrels. The SCT consist of $\sim$16,000 wafers in 4088 silicon modules.The reading is provided by 6 million channels and each channel has its own readout system.

The Transition Radiation Tracker (TRT) is the outermost part of the Inner detector and it is situated in front of the Electromagnetic Calorimeter. The TRT consists of three layers - each has 32 modules. There are 18 endcaps at each side with 224 layers of straws. The TRT is basically a drift-tube with straws parallel to the beam direction which provides the continuous tracking measurement. The straws are placed in the region between 56 cm - 107 cm of the radius and the wires are split in the middle for reducing the occupancy. On the other hand they must be read on both sides so the number of the read-out channels had to be doubled. They are filled with gas mixture of Xe (70%) which is used for absorption of the X-rays, CO_2 (27%) and O_2 (3%). The electrons are identified by the radiator fibres or foils interleaved between the straws themselves.

Figure 12: ATLAS Calorimetry system [Gr3].

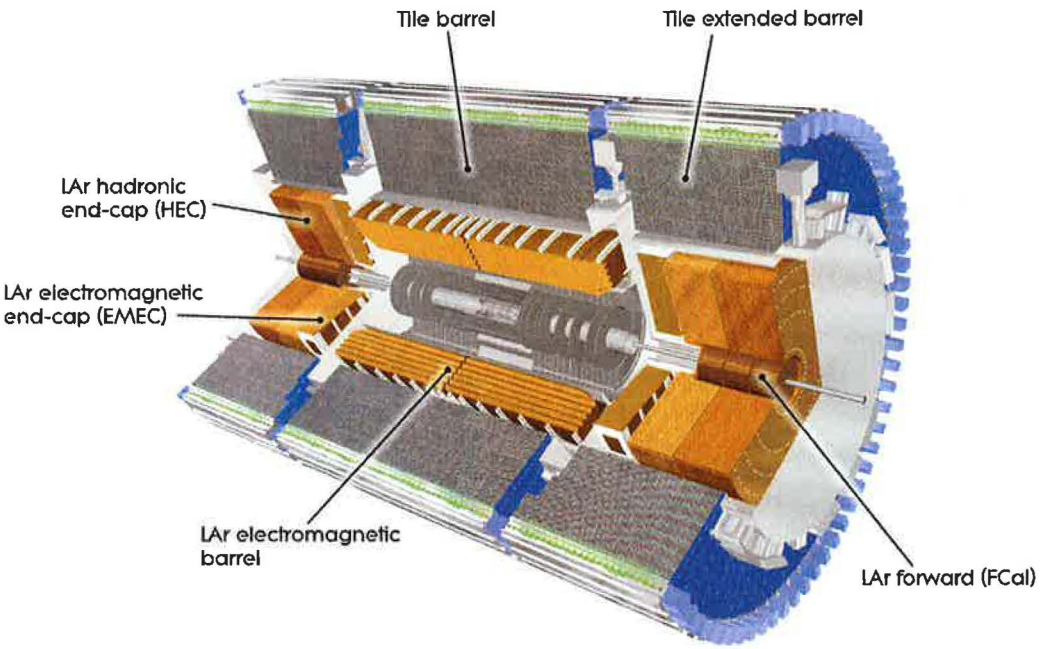

The Calorimeters are set to measure the energy of the particle by the absorption of the particle and corresponding showers. In general calorimeter's energy resolution improves with increasing total energy as

$$\frac{\sigma}{E} = \frac{a}{\sqrt{E}} \oplus b \oplus \frac{c}{E}. \tag{20}$$

The $\oplus$ symbol means that the terms are added in quadratures. The first term is so called stochastic or sampling term which represents general dependency of calorimeter resolution on total energy. It is obvious that for high energies the second term affects the result at most. This term comes from inhomogeneity, bad calibration or non-linearity of calorimeter. The last term stands for instrumental effects. In general a [GeV$^{1/2}$], b, c depend on pseudorapidity η.
The Calorimeters in ATLAS experiment are so called sampling calorimeters which means that the parts used for particle absorption and parts for active read-out are separated. As absorber materials there are used sheets of heavy metals such as uranium, lead or iron which is alternating with active materials (liquid or solid scintillators, proportional counters, etc.). The sampling calorimeters suffers from additional sampling fluctuations and it affects the energy resolution. On the other hand they have good spatial resolution. Even if muons lose their energy only by ionisation it would be possible to measure it. Neutrinos will not deposit any energy in detector at all. ATLAS calorimeter employs so called projective geometry.

The Liquid Argon (LAr) Electromagnetic Calorimeter absorbs energy of particles that interact electromagnetically. The electromagnetic interaction is realised between charged elementary particles and the mediating particle is photon. Electromagnetic shower has quite narrow profile. Its overall size scales with the radiation length which is also defined as

$$\frac{1}{X_0} = \frac{4\alpha N_A Z(Z+1) r_e^2 log(183 Z^{-\frac{1}{3}})}{A}, \tag{21}$$

[FR] where α fine structure constant, N_A Avogadro's number, Z atomic number of the traversed material, A atomic weight of the transversed material and r_e electron radius. The probability of creating an electron-positron by high-energy photon is $7/9X_0$. For the high-energy photons and electrons dominates processes like bremsstrahlung and electron-positron pair production.

The EM Calorimeter is separated into three barrel sections and two endcaps. The active medium is liquid argon which provides fast build-up of a ionisation signal and hence radiation hardness. As absorber is used lead. The EM Calorimeter contains 173312 read-out channels.

Figure 13: Dependency of the absorption length on the pseudorapidity in ATLAS calorimetery system [LAr].

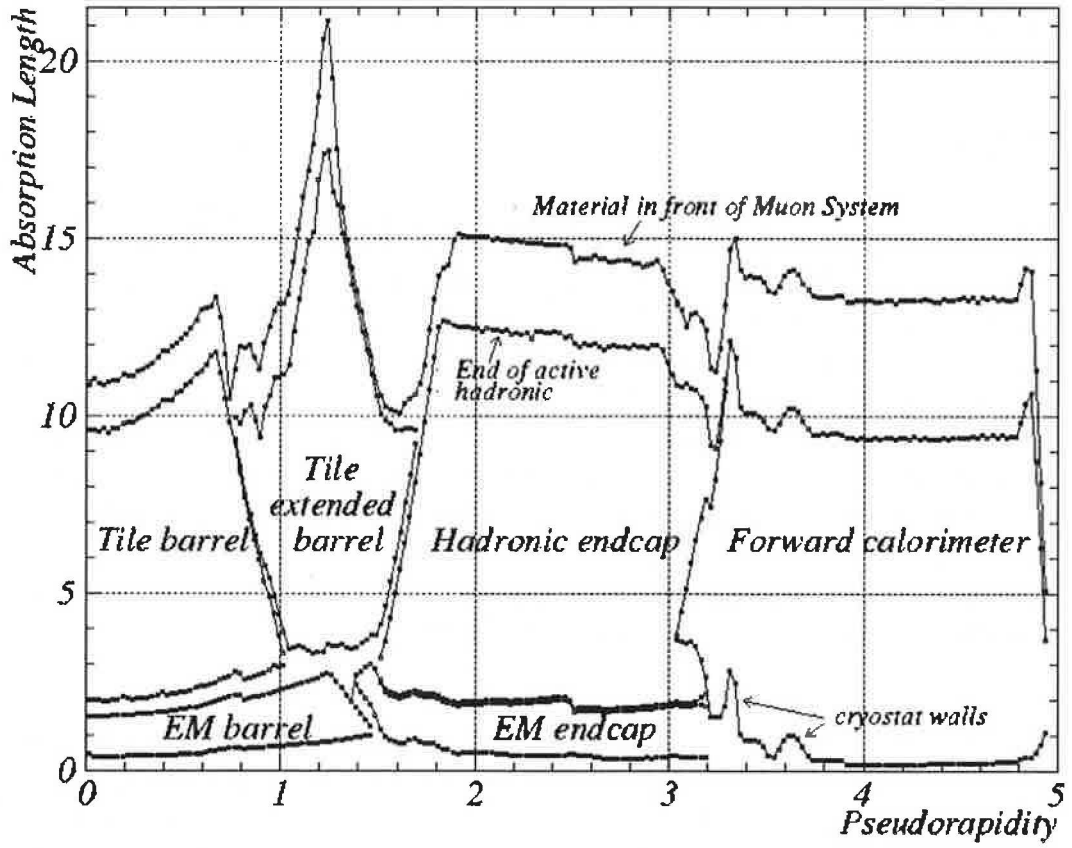

- Electromagnetic Barrel (EMB)
  The EMB is the main detector for measuring electron energy in central part of the ATLAS

detector. If the Higgs boson mass is below 130 Gev the most promising decay mode is $H \rightarrow \gamma\gamma$. If the Higgs boson has energy ~180 GeV then $H \rightarrow Z^0 Z^0 \rightarrow e^+e^-e^+e^-$ and even in this case the electron can have only 10 GeV. So the EMB must detect electrons with wide range of energies. EMB has energy resolution

$$\frac{\sigma}{E} = \frac{10.1\%}{\sqrt{E}} \oplus 0.17\% \tag{22}$$

[EMB].

- Electromagnetic End-cap (EMEC)
  The EMEC is covering a end-cap region in range $1.375 < |\eta| < 3.2$. The EMEC consist of two wheels - one on each side of the EMB. Each wheel is divided into eight modules. The lead plates are mounted in radial arrangement like the spokes of a bicycle wheel. Each end-cap consist of two coaxial wheels which ensure covering of full pseudorapidity range. The energy resolution is

$$\frac{\sigma}{E} = \frac{22\%}{\sqrt{E}} \oplus 0.4\% \tag{23}$$

[EMEC].

The Hadronic Calorimeters

The hadronic shower will be fully absorbed in the Hadronic Calorimeter even if it may start in the Electromagnetic Calorimeter. For hadronic shower is typical wide fluctuating shape. It's only partly determined by the radiation length, which is defined as the mean distance over which a high-energy electron loses all but 1/e of its energy by bremsstrahlung. At most the creation of the hadronic shower depends on nuclear interaction length which is as inelastic cross section a function of energy and type of incoming particle. The interaction length for dense materials is much greater than the radiation length (for iron it is about 17 cm). The problem with high-energy hadronic shower is that the final states may differ. Hence up to 30% of incident energy may be lost due to nuclear excitations and break-ups, spallation of slow neutrons and protons and finally because of undetectable neutrinos and ionizing muons. The hadronic shower contains electromagnetic components because of the frequent production of π_0 mesons which decays subsequently into two photons.

- Calorimeter (TileCal)
  TileCal uses as absorber steel and plates of scintillators as an active medium read out by the wavelength shifting (WLS) fibres. The usage of the radially placed WLS fibers allows creation of the three-dimensional cells so the projective geometry can be applied. It has barrel structure as almost all ATLAS parts and it occupies space of radius between 423 and 564 cm. It consist of three barrels. Each barrel is made of 64 wedge shaped modules. The testbeams and Monte Carlo simulations have proved that the best homogeneity is obtained when the calorimeter is placed behind the electromagnetic compartment and

a coil equivalent to a total of about two nuclear interaction lengths of material[TiCa]. The granularity for other detector's parts is coarser but it has to be sufficient for jet reconstruction and measurement of missing transverse energy E_T. The goal for TileCal is energy resolution (noise is subtracted)

$$\frac{\sigma}{E} \sim \frac{50\% GeV^{1/2}}{\sqrt{E}} \oplus 3\%. \tag{24}$$

- Hadronic Endcap Calorimeter (HEC)
  The HEC is designed to provide coverage for hadronic showers in a range $1.5 < |\eta| < 3.2$. The HEC elements are situated in the end-cap cryostat at the either end of the ATLAS tracking volume. It is a liquid argon calorimeter with absorber plates of copper. The resolution is the same as for barrel parts.

- Forward Calorimeter (FCal)
  It consist of three modules featuring cylindrical electrodes with thin liquid argon gaps. One module with copper absorber is for electromagnetic (FCal1) and the rest (FCal2, FCal3) with tungsten absorbers ensures the hadronic measurements. For read-out from 3524 channels are used low-noise GaAs preamplifiers which are mounted inside cryostat [LAr]. FCal is located in each endcap ~470 cm from interaction point. The FCal provides good measurement of missing E_T at high η and tagging of forward going jets. It will cover showers in the range of $3.1 < |\eta| < 4.9$. The energy resolution for hadrons (noise is subtracted) is set by

$$\frac{\sigma}{E} \sim \frac{95.5\%}{\sqrt{E}} \oplus 7.5\%. \tag{25}$$

  and the requirements are for $a = 35\%$ GeV$^{1/2}$ and for $b = 5\%$. And for electrons the known values are

$$\frac{\sigma}{E} \sim \frac{28.5\%}{\sqrt{E}} \oplus 3.5\%. \tag{26}$$

  and required values are $a = 100\%$ GeV$^{1/2}$ and $b = 10\%$ [LAr].

Muon Spectrometer

One of the channels for Higgs boson decay is $H \rightarrow ZZ$ and $Z \rightarrow \mu^+\mu^-$. Muon Spectrometer is designed to achieve a momentum resolution better that 1% for muon transverse momenta down to 1 GeV [Muon]. It will cover the range of pseudorapidity $|\eta| < 3$. Hence it provides the measurement of spatial coordinates in two dimensions. The spectrometer has one barrel and two end-cap parts on each side. The system of the spectrometer consist of three layers:

Monitored Drift Tube Chambers, Cathode Strip Chambers and Central toroidal air-core magnet. The second coordinate of muon track and the fast muon trriger system is provided by Thin Gap Chamber (end-cap) and Resistive Plate Chambers (barrel).

Monitored Drift Tubes (MDT) are used in the region $|\eta| < 2.4$. Their purpose is precise measurement of particle trajectories. The MDT contains $\sim$ 400,000 tubes in the barrel and endcap chambers. A 3-cm-diameter aluminium tube has Wo-Re central wire with 50 μm diameter. The tubes are filled with Argon-CO_2 gas at 3 bar which reduces diffusion so the resolution is better. This mixture is not so suitable for drift-chamber like for example Ar-Ethan because of non-uniform drift velocity but it is safe in large amounts. Maximum drift time is 800 ns and typical drift velocity about $\sim 2\text{cm}\mu\text{s}^{-1}$. The goal is spatial resolution of $\sim 80\mu$m which is equivalent to $\sim$4ns [MDT].

Figure 14: ATLAS Muon Spectrometer and Inner detector crossed by cosmic event [Muon].

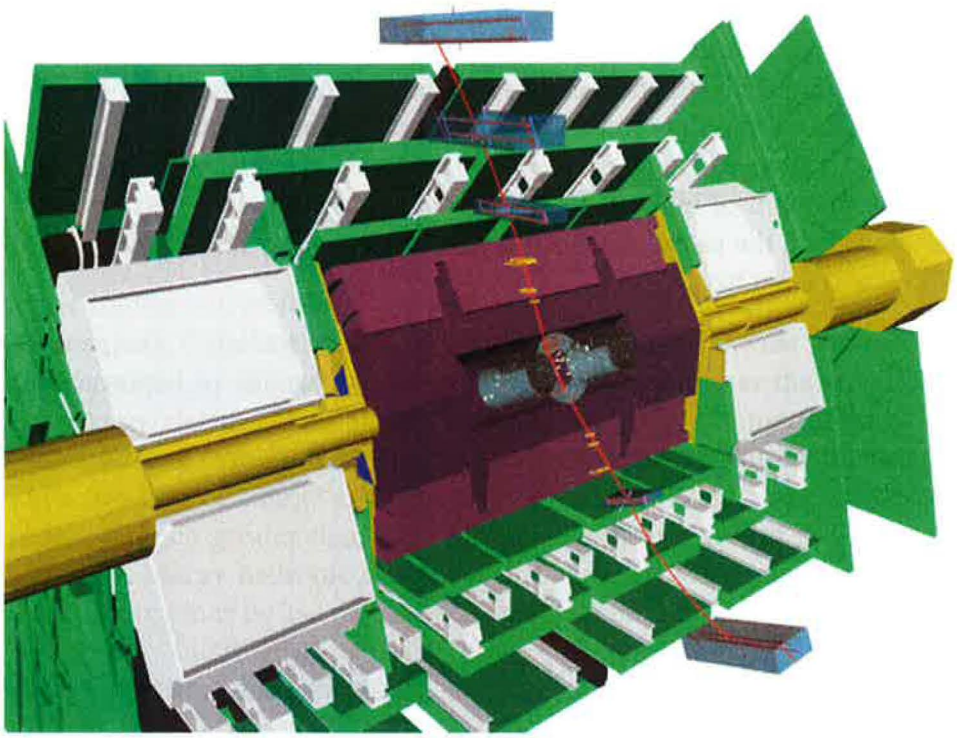

Resistive plate chambers (RPC) are situated in the barrel region and provide trigger and second coordinate information for through going particles. The typical space-time resolution of RPC is 1 cm $\times$ 1 ns with digital read-out. The active element of RPC is narrow gas gap formed by two parallel resistive bakelite plates which are separated by insulating spacers. The efficiency of the RPCs is really high between 97%-98% and with very good time resolution 1.5-2 ns which makes them ideal candidates on muon trigger. To achieve a pure avalanche mode is important to chose a good gas mixture which is Tetrafluorethane, Isobuthane and Sulfur Exafluoride[ARPC].

Thin Gap Chambers (TGC) are used for trigger and measurement of second coordinate in end-caps in region $|\eta| > 2.4$. The TGC design is similar to the multi-wire proportional chamber but the wire pitch is larger than the cathode-anode distance. The anode wires are parallel to the MDT wires and together with the orthogonal read-out strips provide the trigger information. The main purpose of read-out strips is measuring of the second coordinate.

Cathode Strip Chambers (CSC) are used in very forward region of ATLAS because radiation and particle flux there is too high for MDT. It covers the pseudorapidity range $2 < |\eta| < 2.7$. They are the multiwire proportional chambers with cathode strip read-out. The wire spacing is about 2.5 mm.The gas mixture is Ar (30%), CO_2 (50%) and CF_4 (20%). The spatial resolution is better than 60 μm which is achieved by segmentation of the read-out cathode and charge interpolation between neighboring wires [RPC].

ATLAS Magnetic System

ATLAS Magnetic System consist of four parts: two Endcap Toroids (ECT) (see figure 15), one Barrel Toroid (BT) and Central Solenoid (CT) with overall dimensions of 20 m diameter by 26 m length and a stored energy of 1.6 GJ. The total generated field is 2T. This system provides magnetic field for ATLAS Inner and Muon detectors. The magnets are held at temperature of 4.8 K.

Figure 15: ATLAS Toroid magnet [Muon].

The BT are set of eight rectangular 25-meter long and 5-meter wide superconducting coils. It is supplied with a current of 20.5 kA. ECT consist also of eight parts placed around beam axis with offset angle of 22.5°. The CS is a single layer coil situated in a supporting cylinder and enclosed by the cryostat of the Liquid Argon Calorimeter. The magnets are made of Aluminum stabilized NbTi/Cu superconductor, the insulating material is glass tape and fully impregnated with epoxy resin. The cryogenic system is filled with 4.5 K liquid (cooling) and 60 K gaseous (60 K for thermal shielding) helium. [Mag]

2.2 CMS experiment

CMS (Compact Muon Solenoid) has similar goals as ATLAS. The reason for building two devices with similar physics goals is immediate confirmation of discoveries and excluding the systematics. The main distinguishing features of CMS are a high-field solenoid, a full silicon-based inner tracking system, and a fully active scintillating crystals-based electromagnetic calorimeter. ATLAS is in size larger than CMS and has additional Transition Radiation Tracker but CMS is more compact. The momentum resolution would be slightly better at CMS. CMS has solenoidal field of 4T and ATLAS Solenoidal and Toroidal field of 2T. CMS should have better muon momentum resolution. Finally ATLAS has 3-level and CMS just 2-level trigger. The expectations of the CMS experiment are summarized below.

- Good muon identification, momentum resolution over a wide range of momenta ($|\eta| < 2.5$) and good dimuon mass resolution ($\approx$ 1% at 100 GeV.c^{-2}) [CMS].
- Good charged particle momentum resolution and reconstruction efficiency in the inner tracker. Efficient triggering and offline tagging of τ's and b- jets [CMS].
- Good electromagnetic energy resolution, good diphoton and dielectron mass resolution ($\approx$ 1% at 100 GeV.c^{-2}), wide geometric coverage ($|\eta| < 2.5$) [CMS].
- Good E_T^{miss} and dijet mass resolution, requiring hadron calorimeters with a large hermetic geometric coverage ($|\eta| < 5$) and with fine lateral segmentation ($\Delta\eta \times \Delta\phi < 0.1 \times 0.1$) [CMS].

CMS subdetectors

Inner Tracking System

The Inner Tracking System can be divided into two main parts:

Pixel Detector is situated closest to the interaction region and consist of three barrel layers placed in radii of 4.4 cm, 7.3 cm and 10.2 cm [CMS] from the beams and two endcap disks. The size of a pixel is $\sim$ 100 μm $\times$ 150 μm [CMS] to achieve optimal vertex position resolution, giving an occupancy of about 10^{-4} per pixel per LHC crossing. The barrel comprises 768 pixel modules arranged into half-ladders of 4 identical modules each. The spatial resolution is measured to be about 10 μm for the r-ϕ measurement and about 20 μm for the z measurement

[CMS]. The detector readout is using approximately 16 000 readout chips, which are bump-bonded to the detector modules [CMS].

Strip Detectors have as usual barrel and end-cap parts. The barrel tracker region is divided into two parts: a Tracker Inner Barrel (TIB) and a Tracker Outer Barrel (TOB). The TIB is made of 4 layers and covers up to $|z| < 65$ cm [CMS], using silicon sensors with a thickness of 320 μm and a strip pitch which varies from 80 to 120 μm. The endcaps are divided into the Tracker End Cap (TEC) and Tracker Inner Disks (TID). Each TEC comprises 9 disks that extend into the region $120 < |z| < 280$ cm [CMS]. Each TID comprises of 3 small disks that fill the gap between the TIB and the TEC. The TEC and TID modules are arranged in rings, centred on the beam line, and have strips that point towards the beam line, therefore having a variable pitch. The entire silicon strip detector consists of almost 15 400 modules [CMS].

Figure 16: Material distribution of the CMS tracking system [FR].

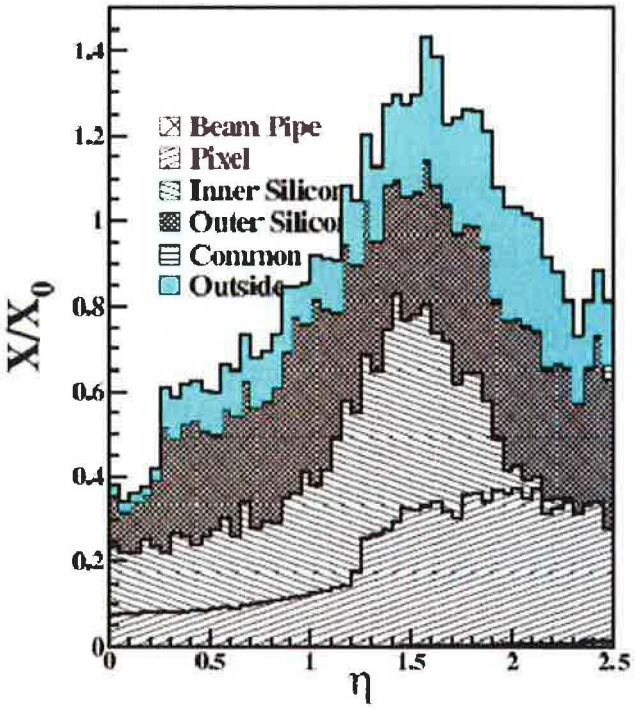

Calorimeter

Electromagnetic Calorimeter (ECAL) is a hermetic, homogeneous calorimeter comprising 61 200 lead tungsten ($PbWO_4$ [CMS]) crystals mounted in the central barrel part (pseudorapidity range $0 < |\eta| < 1.479$), closed by 7324 crystals in each of the 2 endcaps (pseudorapidity

range $1.479 < |\eta| < 3.0$) [CMS]. CMS has chosen lead tungsten scintillating crystals for its ECAL. They have short radiation (X_0 = 0.89 cm) and Moliere (X_m = 2.2 cm) length which is describes a transverse development of the shower due to Coulomb scattering of the electrons and Compton scattering of the photons

$$X_m = X_0 \frac{21.2}{E_c} \tag{27}$$

[Mol]

where E_c [MeV] is the critical electron energy at which the average energy loss due to radiation equals that due to ionization and is given by

$$E_c = \frac{800}{Z + 1.2}, \tag{28}$$

[Mol]

where Z is the atomic number of the target material.The electron shower reaches a maximum when the average electron energy approaches E_c [Mol]. The crystals are fast (80% of the light is emitted within 25 ns) and radiation hard. On the other hand the light yield is 30 γ/MeV which is relatively low. It requires use of photodetectors with intrinsic gain that can operate in a magnetic field. Silicon avalanche photodiodes (APDs) are used as stable photodetectors in the barrel and vacuum phototriodes in the endcaps. Both devices needs for correct operation temperature 0.1 °C.

Hadronic Calorimeter (HCAL) depends on the magnet parameters because most of it is located inside the magnet coil. The HCAl consists of four main parts Hadron barrel ($-1.4 < \eta < 1.4$), Hadron outer ($-1.26 < \eta < 1.26$) [CMS], Hadron endcap ($1.3 < |\eta| < 3.0$ [CMS]) and Hadron forward. The important requirements of HCAL is to minimize the non-Gaussian tails in the energy resolution and to provide good containment and hermeticity for the E_T^{miss} measurement. Maximum amount of absorber is situated under the magnet which keeps minimum space for active medium, referred to as the Hadron outer, so the tile/fibre technology was chosen. It consists of plastic scintillator tiles read out by embedded wavelength-shifting (WLS) fibres.

Muon Chambers

Centrally produced muons are measured three times: in the inner tracker, after the coil, and in the return flux. Momentum measurement of muons using only the muon system is essentially determined by the muon bending angle at the exit of the 4 T coil, taking the interaction point (which will be known to ~ 20 μm) as the origin of the muon. The resolution of this measurement is dominated by multiple scattering in the material before the first muon station up to p_T values of 200 GeV/c, when the chamber spatial resolution starts to dominate. For low-momentum muons, the best momentum resolution (by an order of magnitude) is given by the resolution obtained in the silicon tracker.

There are three types of gaseous detectors. The choice of the detector technologies has been driven by the very large surface to be covered and by the different radiation environments. In

the barrel region ($|\eta| < 1.2$) are used the drift tube chambers (DT). In the two endcaps, cathode strip chambers (CSC) are deployed ($|\eta| < 2.4$ [CMS]). In addition to that, the Resistive Plate Chambers are used in both the barrel and the endcap regions. RPC provide a fast response with good time resolution but with a coarser position resolution than the DT or CSC. RPC can therefore identify unambiguously the correct bunch crossing [CMS].

Figure 17: CMS Muon momentum resolution [FR].

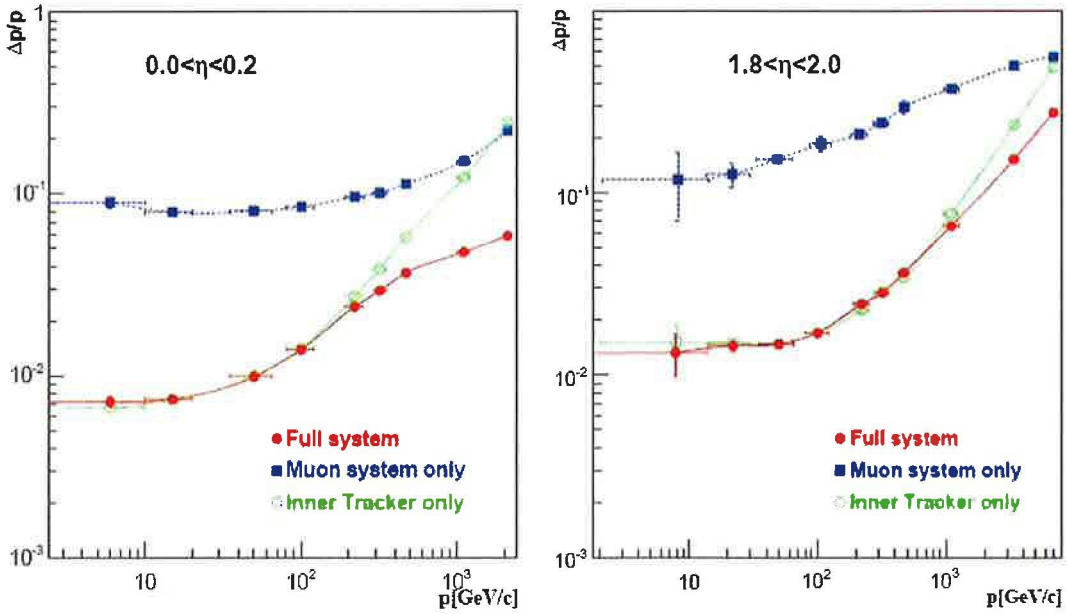

CMS Magnet

The important difference between ATLAS and CMS is the magnet. For CMS was chosen the large superconducting solenoid. With given parameters

Table 5: Parameters of the solenoid [CMS].

Field	4 T
Inner Bone	5.9 m
Length	12.9 m
Number of Turns	2168
Current	19.5 kA
Stored energy	2.7 GJ
Hoop stress	64 atm

A large solenoid can obtain high bending for a good momentum resolution. For good momentum resolution in the forward region is necessary optimum

length/ radius ratio. The main features of the solenoid are high-purity aluminium-stabilised conductor and indirect cooling (by thermosyphon) and full epoxy impregnation. A conductor with larger cross-section (64 mm × 22 mm) can withstand an outward pressure (hoop stress) of 64 atmospheres. The conductor carries a current of 20 kA. The mass of a particle can be determined from its momentum and speed. The momentum of a charged particle is measured by its deflection in a magnetic field. The purpose of the RICH detectors is to match up this information with a measurement of the particle's speed[CMS].

Figure 18: Dependency of the Higgs boson mass m_H on statistical significance of higgs production processes [CMS].

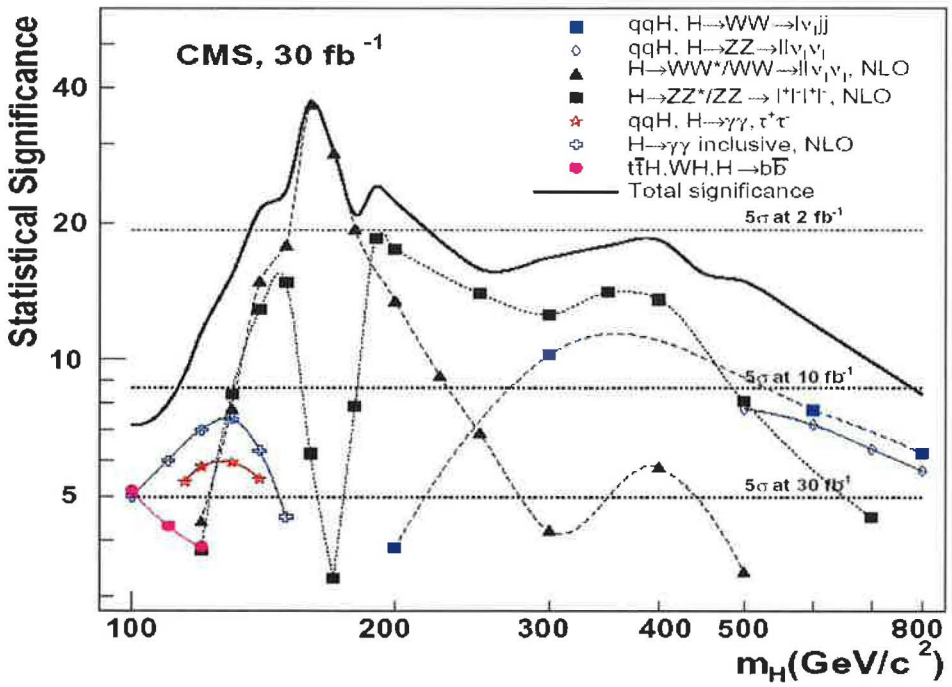

2.3 ALICE

ALICE (A Large Ion Collider Experiment) is an experiment for studying the heavy ion collisions, at a centre-of-mass energy per nucleon pair of 5.5 TeV and the Quark-Gluon Plasma that will be formed in this process [ALDR].

Inner Tracking System

The Inner Tracking System (ITS) provides measurement of the primary and secondary vertexes positions and low momentum particles. In heavy-ion collisions a special ITS design is required because the particle density is extremely high. Closest to the beams are situated the the Silicon Pixel Detectors (SPD). They provide spatial and two-track resolution in bending plane. The SPD has a basic unit called a ladder which contains silicon sensor and five pixel

Figure 19: ALICE detector [Gr3].

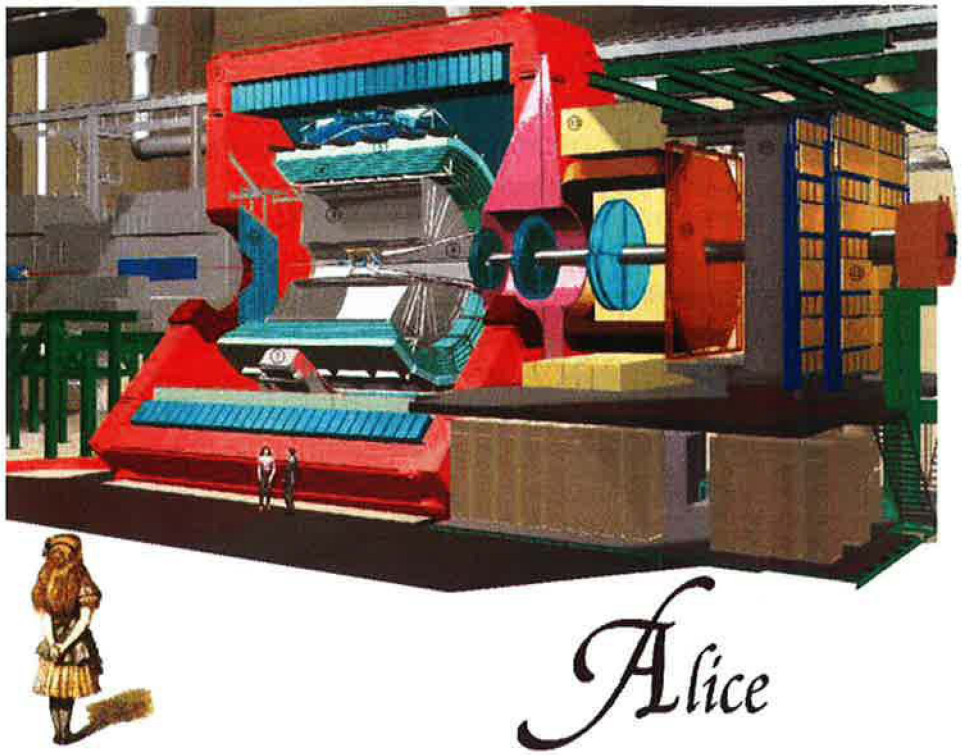

chips. The follow-up two layers are Silicon Drift Detectors (SDD) which are mounted on a ladder structure. The two outer layer are composed of double sided Silicon Strip Detectors (SSD) [ALDS].

Time Projection Chamber

The Time Projection Chamber (TPC) is a main part of the ALICE detector. It provides measuring of charged particles momentum with very high precision for values below 10 GeV/c but as it is a part of tracking system it has good resolution up to 100 GeV/c. For measurement's accuracy is important precise determination of the energy loss. The resolution in this measurements is predicted to be about 5-6 % at a particle density below 2000 per unit of rapidity and about 7 % at 4000 particles per unit of rapidity. [ALDS] The ALICE has a cylindrical shape and it is divided by the central electrode in two regions so the drift volume is defined by the two field cage vessels and covering radii from 0.9 m to 2.5 m. As a drift gas to fill is used mixture of Ne (90%) and CO_2 (10%) [ALpo]. The charged particles ionize the gas, the electrons drifts to the anode wires and the positive ions induce a positive signal on some of the 570132 cathode pads [TPC].

Particle Identification Systems

The Particle Identification System (PID) is a crucial part of the ALICE detector. The central tracking is provided by TPC through energy loss measurements and ITS discrimination of π/K/p in the non-relativistic regime. The central tracking detector gives the identification of short-lived particles through their hadronic decays and provides the vertex finding [ALDS]. There are several complementary detectors which belongs to the PID.

Transition Radiation Detector (TRD) provides ITS and TRD the high-momentum electrons identification and pions discrimination. TRD can operate as spectrometer and it measures i.e. charm and beauty through their semi-leptonic decay. The TRD is very fast tracking detector that's why it is used for triggering of high momentum electrons and hadrons [ALDS].

Time-Of-Flight Detector (TOF) is based on Multi-gap Resistive-Plate Chambers (MRPC). TOF plays important part in the identification of the kaons, pions and muons in the momentum range 200 MeV/c - 2.5 GeV/c [ALDS].

High Momentum Particle Identification Detector (HMPID) is based on Cerenkov ring-imagining and covers limited rapidity range (-0.6 < η < 0.6). The radiator is liquid and multi-wire proportional chamber with pad readout. The HMPID extends the he range of identifying and separating charged hadrons towards higher p_T, 3 GeV/c for π/K and 5 GeV/c for K/p [ALDS].

Photon Spectrometer (PHOS) is high segmented $PbWO_4$ calorimeter for high resolution pions and photon measurements to identify the neutral mesons through their two-photon decay channel and for discrimination against leptons and charged hadrons. The detector for excluding the charged particles is placed in front of the PHOS and is based on multi-wire proportional chambers [ALDS].

Muon Spectrometer

Complex spectrometer for muon identification is placed in the forward region. At high temperature or energy density, above c = 0.7 GeV.fm^{-3} or $T_c \sim 180$ MeV [ALMS], lattice calculations of the quantum chromodynamics (QCD) predict a transition of nuclear matter from a hadron gas to a quark–gluon plasma (QGP). The design of the muon spectrometer was driven by the requirement of searching for these complicated processes which can be hard to find in the large background environment of central Pb–Pb collisions [ALMS]. The spectrometer acceptance covers the angular range of $-4 < |\eta| < -2.5$ [ALMS]. The spectrometer consists of a complex hadron absorber, a 3 Tm dipole magnet, 5 planes of tracking chambers and 2 planes of trigger chambers [ALDS].

Forward Detectors

ALICE will have various detector systems at large rapidities on both sides of the interaction point. These detector systems will provide information for triggering, event selection and global properties. The Forward detector consist of five parts [ALMS].

The Zero Degree Calorimeters (ZDC) is mostly made of tantalum or brass with embedded quartz fibers [ALMS]. ZDC provide trigger information and determine the impact parameter.

The Photon Multiplicity Detector (PMD) is located 3.6 m from the interaction point on the opposite side to the muon spectrometer [ALMS]. It composes of proportional chambers sandwiching a passive Pb converter. The detector measures photons and charged particles at large rapidities. PMD searches for non-statistical event-by-event fluctuations and flow.

The Forward Multiplicity Detector (FMD) consist of 5 discs of Si pad detectors, two of them are situated on the muon spectrometer side and three on the opposite side. The FDM with the Inner Tracking System covers the wide range -5.1 < $|\eta|$ < 3.4 for charged particle measurements [ALMS].

T0 system is based on Cherenkov radiator and Photomultiplier tubes. The goal of the T0 detector system is to provide the start signal for the time-of-flight measurements as well as a signal for the L0 trigger with a time resolution better than 50 ps.

V0 system consists of two arrays of scintillators embedded with wavelength shifting fibres. The arrays are placed on each side of the interaction point (90 cm on the muon side and at 355 cm on the opposite side). The V0 system provides the main interaction trigger and online vertex position determination.

2.4 LHCb

LHCb (Large Hadron Collider Beauty) is an experiment especially developed for for b-physics. The main goal is measuring the parameters of CP violation in the interactions of b-hadrons. The crucial part of the LHCb detector are RICHs (Ring imaging Cherenkov detectors) which are designed to distinguish kaons and pions. The tracking system is placed before and after the dipole magnet.

RICH system

To determine mass of the particle is needed to measure momentum and speed The momentum is measured from its deflection in magnetic field. RICH (Ring Imaging Cherenkov) detector determines its speed from the angle of Cherenkov photons emission.

Every time a charged particle travels through material with a velocity v greater than a velocity of light in that medium then it emits a Cherenkov radiation. It is caused by molecules polarized

Figure 20: The LHCb detector scheme [Oxf].

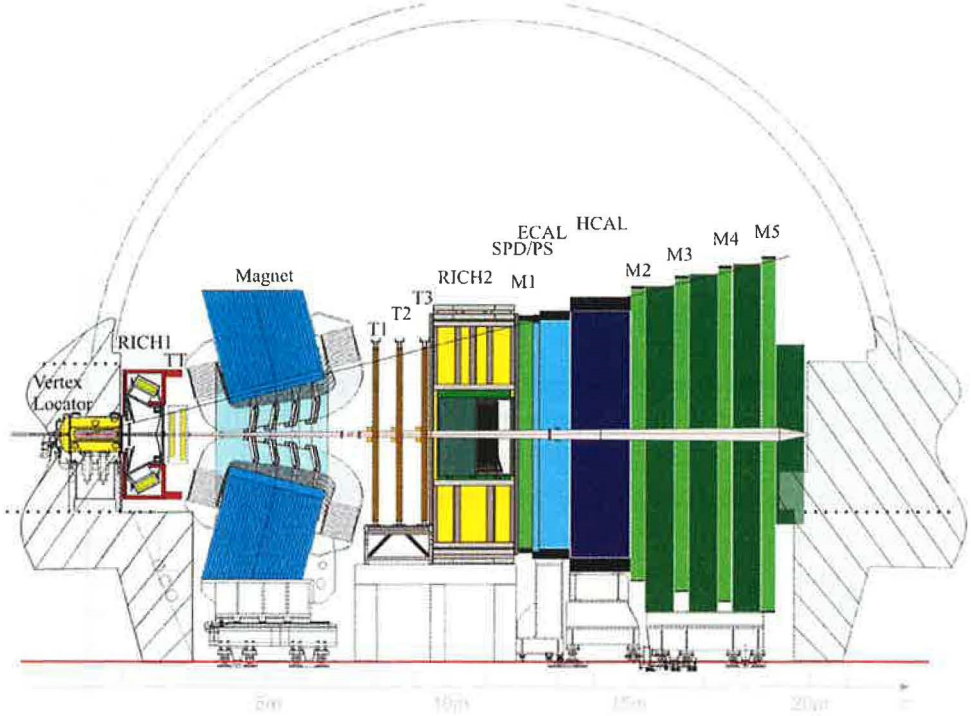

by the come-along charged particle which emits photons to get to their ground state. Cherenkov light is emitted under a Cherenkov angel θ (the angle between the emitted Cherenkov radiation and the particle path)

$$\cos\theta = \frac{1}{n\beta}, \tag{29}$$

where n is refractive index of the material and $\beta = v/c$. So the maximum angle is for $v = c$. The Cherenkov radiation has modest light output which means that energy loss due to ionization or excitation are much higher (two or three orders of magnitude). But with the help of the photomultiplier with suitable wavelength-sensitivity the Cherenkov radiation is possible to separate it from background. The photon yield is obtained by

$$\frac{dN}{dl} = 2\pi\alpha\left(1 - \frac{1}{n^2\beta^2}\right)\int\frac{d\lambda}{\lambda^2}, \tag{30}$$

where N is number of photons, α fine structure constant, λ wavelength, l length of traversed radiator [Oxf].
The Cherenkov photons are reflected out by mirrors and travels to an array of photodetectors. These photons are reflected by mirrors, out of the region where particles are travelling through the detector, to an array of photodetectors. This reduces the amount of material the particles travel through before reaching the last stages of the detector and protects the photodetectors from the large magnetic field and high radiation level. The photons produce a ring of hits on

the photodectors, and the radius of this ring plus the reconstructed track is used to identify the type of particle [Oxf].

LHCb has chosen to use Hybrid Photon Detectors (HPDs). This technology, developed at CERN, satisfies the LHCb requirements of high sensitivity to single photons and fast readout speed. The readout time has to be compatible with the 25 ns between LHC bunch crossings. The photodetector planes will cover a total area of 2.6 m^2 with a granularity of about 2.5 mm $\times$ 2.5 mm [RICH]. The LHCb detector includes two RICH counters which provide charged particle identification over the momentum range from 1 - 150 GeV/c. An upstream detector is RICH 1 and it contains the aerogel and and C_4F_{10} radiators, covering the full outer acceptance of LHCb [RICH]. The RICH 2 is placed between 9450 mm $\leq z \leq$ 11900 mm. It is placed between the last tracking station of the spectrometer and the first muon station. RICH 2 will track the high-momentum tracks which will traverse the magnet. The Cherenkov medium is CF_4. It is operated at atmospheric pressure and at room temperature.[RICH2]

Tracking system

The tracking system measures trajectories of the charged particles and their momentum. It is placed before and after the dipole magnet. Closest to the beam is the Vertex Locator (VELO). It needs to be hold in vacuum. VELO is a silicon microstrip detector measuring the coordinates R and ϕ coordinates of the particle. The Trigger Tracker (TT) is located between the VELO and the magnet. This detector obtains an estimate of the momentum and has a big importance for the trigger decision. The TT is a silicon strip detector with a pitch of 183 μm. Behind the magnet the tracking station consist of two types: the silicon strip detectors which are situated in the inner region and the outer region is covered by straw tube chambers diameters of 5 mm. [TS]

Calorimeter system

The calorimeter sub-detectors in LHCb are the Scintillator Pad Detector (SPD), the Preshower detector (PS), the Electromagnetic Calorimeter (ECAL) and the Hadron Calorimeter (HCAL). The HCAL is situated at 13.33 m from the interaction point. It has extremely similar structure as ATLAS TileCal. Its instrumented depth is 122 cm. HCal has no longitudinal segmentation. It is supposed to provide $\sim$70% of Level-0 trigger output. The purpose of LHCb calorimeter system is to ensure the fast trigger system thanks to the fast identification of high transverse energy electron, photon, π^0 and hadron candidates. The other thing is the offline identification of electrons and the reconstruction with a good accuracy of prompt photons and π^0's for physics analyses.

Muon system

There are five tracking systems along the beam axis. The 48% of the detector is occupied by the Muon system. The first one called M1 is upstream (12.1m from the interaction point) and M2 - -M5 downstream (15.2m - 18.8m) the Calorimeter. The main tasks for the muon detector are the function as high-p_T muon Level-0 trigger and offline muon identification [MTDR].

Originally the Resistive Plate Chambers were supposed to be installed in the outer region but the problem with their aging occurred [ATDR] so the Muon Stations (480 double-gap chambers) M4 and M5 were installed. In front of the Calorimeter preshover is placed 12.1 m from the interaction point the M1 station. It provides transverse-momentum measurement of the muon tracks. The remaining four stations are interlard with the muon shield which comprises of the ECal, HCal and iron filters [MTDR].

2.5 Smaller experiments at LHC

TOTEM experiment

A precise measurement of the total pp cross-section σ_{tot} elastic scattering has importance for distinguishing between different models of soft proton interactions. The large uncertainties of the cosmic-ray data and the standard-deviations discrepancy between the two final results from the Tevatron make an extrapolation to higher energies uncertain. It leaves a wide range for the expected value of the total cross-section at energy of $\sqrt{s}$ = 14 TeV. From 90 to 130 mb, depending on the model which was used for the extrapolation. Biggest contributor to this total cross section number the inelastic scattering, then elastic and just several percents fall on diffractive scattering. The TOTEM collaboration at CERN is focused on studying total, elastic and diffractive dissociation of proton–proton cross sections at the maximal accelerator energy [TOT].

At an early stage with non-optimal beams, TOTEM will measure the total cross-section and the luminosity with a precision of about 5% [TOT]. After having understood the initial measurements and with improved beams a precision will approximately 1% should be achievable [TOT]. TOTEM will measure σ_{tot} and the luminosity L simultaneously by taking advantage of the optical theorem according to (16) and (17).

The importance of TOTEM lies in its detector systems which have trigger capability for CMS. A flexible trigger can be provided by the Roman Pot detectors and the T1 and T2 telescopes. TOTEM will take data under all optics conditions, adjusting the trigger schemes to the luminosity. The DAQ will allow trigger rates up to a few kHz without involving a higher level trigger [TOT].

LHCf experiment

LHCf is the smallest experiment of the six official LHC experiments. It is installed near the ATLAS experiment. The goal of the LHCf experiment is studying the neutral-particle production cross sections in the very forward region of proton-proton and nucleus-nucleus interactions. Neutral pions, gammas and neutrons production will be investigated during the initial phase of the LHC running because of the luminosity below $10^{30}\text{cm}^{-2}\text{s}^{-1}$ [LHCf2]. This experiment should give an understanding of the development of atmospheric showers in the Earth atmosphere induced by the very high energy cosmic ray. The prediction of the shower development depends on the interaction models and it is important to get real data and compare them with the models. The main problem is that there is the the uncertainty of cosmic-ray spectrum

composition between 10^{15}eV and 10^{19}eV [LHCf2]. LHCf consists of two imaging and sampling calorimeters made of tungsten plates, plastic scintillator and position sensitive sensors. Both detectors are similar with different geometry and different tracking systems.

The fist detector consists of three towers with the same longitudinal structure but with different transverse dimensions. Absorber material is tungsten and there are used plates with different thickness (7 mm – 14 mm). Different towers dimension - the small one close to the beam, big one far away from the beam - minimize the multihit events. The scintillators are fibers which provide transverse shower profile measuring and triggering [LHCf].

The second detector uses silicon microstrips detectors 70×70 mm^2 with a pitch 80 μm^3. The microstrip detectors provide better impact point measurement, selection of clean events (just one γ) and π^0 mass reconstruction (energy calibration). Energy is measured by counting the secondaries [LHCf].

Calorimeters are installed 140 m away from the interaction point, in front of luminosity monitors inside the TAN (Target Neutral Absorber) [LHCf2]. The TAN is massive zero degree neutral absorber located in the proximity of the interaction point (IP) 1 to protect the outer superconducting beam separation dipoles from neutral particle debris from the IP. Charged particles from the IP are swept aside by the inner beam separation dipole D1 before reaching the TAN [LHCf2].

3 Data Acquisition and trigger architecture of ATLAS

3.1 Trigger motivation

The high bunch-crossing rate and the large number of read-out channels ($\sim 10^8$) makes from ATLAS Trigger and Data Acquisition system a real challenge. The initial bunch-crossing rate is needed to be reduced on about 200 Hz ($\sim$ 23 events per bunch crossing) while the interesting data must be preserved and separate the extremely high rate of the background events. It can be summarised that trigger must be trigger, flexible and robust.

Figure 21: The number of background events in contrary to interesting ones and their dependency on the cross-section [Mol].

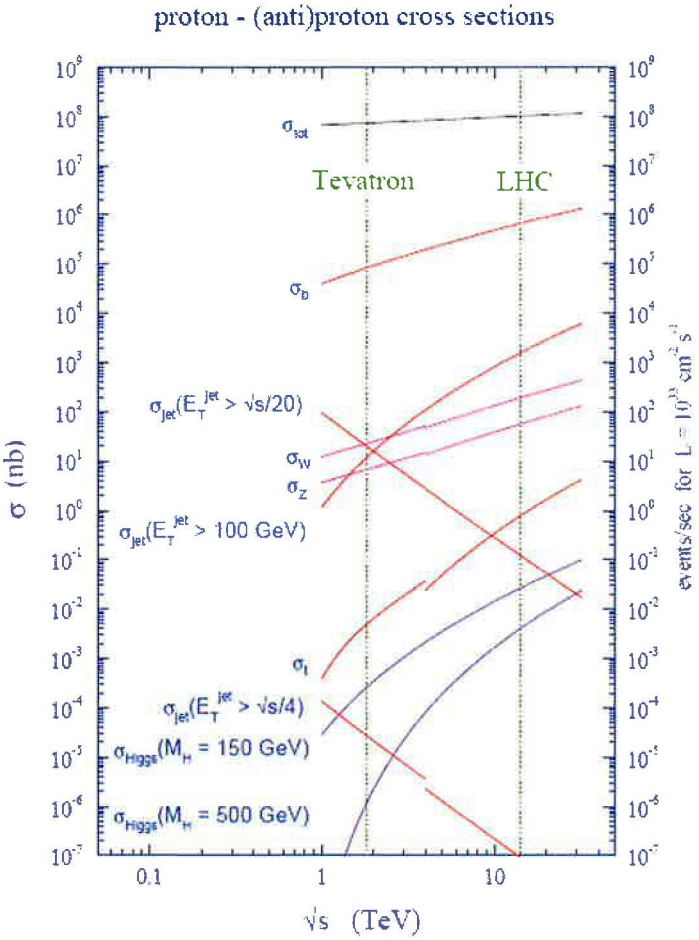

The ATLAS has three-level trigger system where the first one is implemented in hardware. The second and third level is called the High Level Trigger and they are implemented in software. The physics trigger expectations are

- Cover all topologies expected from new physics
- Sensitivity to presently unknown new physics

- Keeping safety margin against uncertainties
- Possibility to refine/optimize selections offline with more powerful analyses

3.2 Trigger architecture

Figure 22: Trigger architecture [TW].

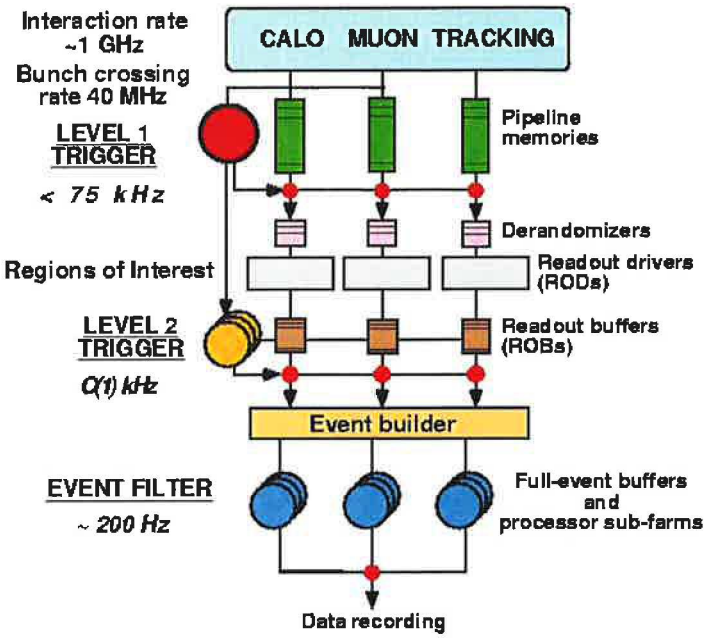

HLT/DAQ system consists of four main parts:

- The Data flow system - receiving detector data, serving of a subset of data to the HLT system, transport of selected event's data. to mass storage
- The HLT system — responsibility for the post-LVL1 event selection and filtering and classification of all accepted events.
- The Online system — responsibility for all aspects of experiment and TDAQ operation and control during data taking, during testing and calibration runs.
- The DCS (Detector Control System) — provide the coherent and safe operation of the ATLAS detector, the interface with external systems and services including the LHC itself.

A short list of used terms

For more detailed description and more terms see [TW].

The Data Acquisition System: The system comprising the Data Flow, Online and Detector Control System.

Data Flow Manager (DFM): An element of the event building sub-system which ensures the correct flow of data between event builder sources and destinations.

Event: All the Read-Out Buffer (ROB) fragments from the same bunch crossing.

Event data fragment: A generic term for a sub-set of event data. Specific instances of an event fragment are ROD, ROB, ROS and sub-detector fragments.

Event Builder: Part of the Data Collection sub-system, it merges all the fragments belonging to a unique L1ID into a full event at a single destination.

Event Filter (EF): The hardware and software required for the final stage of the on-line event selection, data monitoring and calibration using offline style algorithms operating on complete events accepted by LVL2.

Read Out Buffers (ROBs): A sub-system of the ATLAS TDAQ responsible for reading out the ATLAS RODs and for supplying event fragments to the LVL2 and EB sub-systems.

Read-Out Driver (ROD): The ROD gathers data from the derandomizers over one or more data streams and builds ROD fragments of events to be sent to the ROS or the RoIB. It gathers data from Front End Boards (FEBs) and then sends fragments to ROB or RoIB.

Region of Interest (RoI): A region limited in eta and phi, indicated by the LVL1 trigger to contain candidates for objects requiring further computation. In the case of B-physics triggers at low luminosity, some ROI's may be defined internally within the level-2 trigger system.

Region of Interest Builder (RoIB): The element which combines RoI information from different parts of LVL1 and forwards it to a LVL2 supervisor.

Read-Out Links (ROL): The physical link between ROD and ROS through which the data are sent at the rate of the LVL1 trigger.

Read-Out System (ROS): A sub-system of the ATLAS TDAQ responsible for reading out the ATLAS RODs and for supplying event fragments to the LVL2 and EB sub-systems.

Trigger System, Data Acquisition System and Data Collection System (TDAQ): The abbreviation for the complete ATLAS trigger project. It comprises the three level Trigger System, Data Acquisition System and Data Collection System.

Sub-Farm Imput (SFI): Part of the data collection sub-system. The location where full event are built by the EB. Some of the other terms will be explained in the text below.

The Data Flow system

"The boundary between the detector readout and the data acquisition is at the input of the Read Out Buffers (ROBs). The Read-Out Links (ROLs) is the physical link between Read-Out Driver (ROD) and Read-Out System (ROS) through which the data are sent at the event rate of the LVL1 trigger. The Read-Out System (ROS) contains several Read-Out Buffers (ROBs). Requested data fragments from selected ROBs are served to the LVL2 trigger element of the HLT system. Event data fragments for LVL2-accepted events are then built, on the initiation of the Data Flow Manager (DFM), from the ROBs, across a switched Ethernet network, into a complete event by one of the ~100 Sub-Farm Inputs (SFIs). The SFIs then serve the complete events to the second element of the HLT system, the Event Filter (EF). Events selected by the EF for final archiving in preparation for offline reconstruction and primary analysis are passed to permanent storage via the final element of the Data Flow system, the Sub-Farm Output (SFO). Most of the element interconnection in the Data Flow system is done using standard gigabit Ethernet network and switching technology. The maximum network bandwidth capacity required for building events accepted by the LVL2 trigger is expected to be 5 Gbyte/s, much less than the aggregate data rate into the RODs for events retained by LVL1."[CTDR]

The HLT system

The HLT trigger comprise LVL2 trigger and the Event Filter (EF). Both use farms of PCs connected by ethernet network. The importance of LVL2 trigger is in high rejection power and fast algorithms with limited precision. On the contrary the Event Filter has modest rejection power and very precise algorithm which means that they are more time and computing power demanding.

RoIs seeded by LVL1 trigger are processed by LVL2 trigger. So the event processing time is about 10 ms. That's why LVL2 trigger uses a highly optimized selection algorithms. One of the goals of LVL1 trigger is to identify the Regions of Interest (RoI). Then Regions of Interest Builder (RoIB) puts together the information about RoIs and sents it to the LVL2 Supervisor (L2SV). LV2S supervisor is responsible for distributing the events to the LVL2 farms and subfarms and then computing on the allocated processors the final LVL2 decision. These results are passed via L2SV to the Data Flow Manager (DFM) and based on the decision are the events build or flushed from the Read-Out System memory. The data are stored in ROBs during the LVL2 processing until the event building process is completed.

The Event Filter works at the LVL2 acceptance range which means that event treatment time is about 1 ms and the output rate is ~200 Hz. The EF receives the fully build events from Sub-Farm Input (SFI) which is the part of the data collecting subsystem. It uses the full detector granularity with potential full event access to offline algorithms. The EF algorithms are more sophisticated than those used in LVL2 trigger. It provides the online event selection, data monitoring and calibration. Events which did not pass are disscarted, accepted ones are sent to the Sub-Farm Output (SFO) to mass storage.

The Online Software system

It serves to configuring, controlling and monitoring the TDAQ system. But it does not include any management, processing or transportation of the event data. Its function is to starting up and shutting down, synchronization and supervision of the entire TDAQ system.

The Online Software System includes for example the Message Reporting System (MRS) which provides for all software components of the TDAQ system reporting error messages to other components or the Process Manager (PM) which performs the basic job control like starting, stopping and monitoring of basic status of software components of the TDAQ.

The Detector Control System

The DCS provides supervision of all hardware of the experiment set-up, including all detector systems of ATLAS and the common experimental infrastructure. Hence some parts of the detector works continuously and so the DCS in contratry to DAQ which runs only when needed. The other function is to communicate with external systems like the infrastructure services of CERN (cooling, ventilation, electricity distribution, alarm system etc.) and LHC. The operators communicates with the detector via DCS. The DCS is the only part of Trigger system that holds the safety responsibility. This concerns mainly looking over the risk before allowing certain procedures to be executed. The DCS can take some actions automatically (f.e. in case that the detector can be damaged).

The data of a good quality demand precise synchronisation of the DAQ and DCS. DAQ deals with the data describing a physics event (characterized by an event number) and the DCS treats all data connected to the hardware of the detector (operational state of the detector when the data were taken) and categorize them by a time interval. The correlation between both sets of data is crucial for offline analysis.

3.3 Data types

The data types varies as the tasks of the TDAQ parts differs. Here is a very brief description [CTDR]

- Detector Control Data

  This data will be produces by the DCS. Mostly they will consist of hardware-parameters and system statuses. The rate of this kind of data will be $\sim$1 Hz. It's expected that these values will not vary very much in the time periods.

- Byte-stream

  Data which flow out of the trigger.

- Event Data

  Event data are data read out from the detectors and data produced by various stages of the trigger while processing the event.

- Configuration data

  Configuration data are used to prepare the TDAQ and detector systems for data-taking which includes configuration of the system for particular run. Even a data-taking run is defined by set of a given configuration data.

- Conditions Data

  Includes some data from the above-mentioned categories. Conditions data are data that are needed for complete analysis of any given selection of event data.

- Online statistic and monitoring data

  Quite similar to DCS data. This data will be produced by detector and TDAQ system during data taking. The importance of this data type lies in possible observation how different parameters vary.

For purposes of this thesis are important just the Event Data types.

Event Data Model

The Event Data Model (EDM) includes different data formats [TW]:

- RDO (Raw Data Object)

  The data from ROS and trigger system are in Byte-stream format which reflects the format in which the data are delivered from the detector. The byte-stream information is represented by RDO which is a C++ object representation. The RDO files are read by the reconstruction algorithms. The nominal size of RDO data is $\sim$ 1.6 MB/event [TW].

- ESD (Event Summary Data)

  Processed (for example calibrated and reconstructed) raw data are put into ESD format. It contains the detailed output of the detector reconstruction and some information about hits and clusters. The access to the ESD files is not allowed for the normal user. The nominal size of ESD data is $\sim$ ESD 1.0 MB/event [TW].

- AOD (Analysis Object Data)

  Next reduction is to the AOD format. AOD is the summary of event reconstruction and contains physics objects. The information in an AOD file is organized in containers. There is a key which is needed to get at it. The list of the AOD containers and keys is available at the [TW]. The container name and the access keys are usually the same for the AOD and the ESD. The list of the objects of the AOD containers. For example the Event information container contains the EventInfo object that provides access to the basic information about the type (EventType), trigger information (TriggerInfo) and identity (EventID). The nominal size of AOD data is $\sim$ 100 kB/event [TW].

- DPD (Derived Physics Data)

  DPD contains derived data from AODs, Conditions data and slimmed events information. Physics groups usually produce their own DPDs. The nominal size of DPD data is $\sim$ 10 kB/event [TW]

- TAG

  Database or ROOT files which are used to quickly select events in AOD and/or ESD files. The nominal size of TAG data is $\sim$ 1 kB/event [TW].

Figure 23: The data processing and reduction of their given nominal sizes [TW].

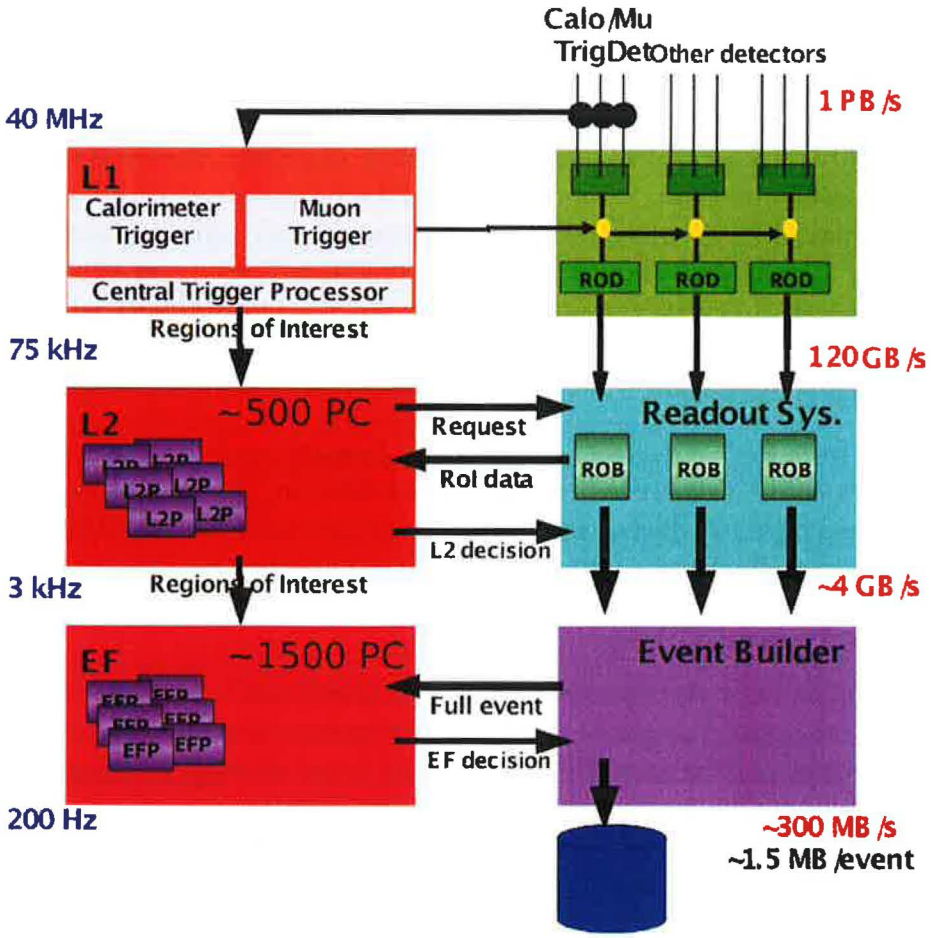

3.4 ATLAS Computing

The processing of ATLAS Data is done on the Grid.

ATLAS Computing Model

Tier-0/CAF

Tier-0 facility is located at CERN. The goal of Tier-0 is to archive data to CERN Castor Mass Storage System tape and distribute the primary RAW data received from the Event Filter (EF) for storage and subsequent reprocessing to Tier-1 Facilities. The data must be copied in case of error or malfunction of Tier-0. Tier-0 runs the first-pass calibration (within 24 hours) and first-pass reconstruction (within 48 hours). The first-pass processing is bytestream RAW data and the output is ESD. After that derived databases (ESDs, DPDs, AODs ...) are sent from Tier-0 to Tier-1 facilities. CAF provides access to Raw data. No simulations are run there. Its purpose is to work on algorithmic development, calibration and alignment.

Tier-1

Tier-1 consists of 10 facilities all over the world. It's purpose is to store and provide access to fractions of RAW data. They provide capacity to perform reprocessing of RAW data. They rerun reconstruction with better calibration/alignment and/or algorithms. Then the reconstruction outputs are distributed to to Tier-2 Facilities. Next they keep current versions of ESDs and AODs for analysis. Finally they run event selection and jobs analysis on a large scale.

Tier-2

Tier-2 Facilities provides calibration, simulation and analysis. They provide analysis capacity for physics groups. At the stage of the Tier-2s current versions of AODs and samples of other data types are kept. There will be about 35 facilities worldwide.

Tier-3

They ensure access to Grid resources and local storage for end-user data. Tier-3 Facilities are in general represented by resources not for general ATLAS usage (local university clusters, desktop machines...).

3.5 ATLAS Online Computing

The online software is set of software/framework for configuring, controlling, and monitoring the TDAQ. By the help of Online software users can communicate with TDAQ system and control the status and performance of the TDAQ system. It allows the user to configure and control the data taking operation. Other important thing about Online Software is that it provides right synchronization for the states of a run and performing start-up and shut-down procedures. The online software does not contain the management, processing, and transportation of physics data. For this thesis Offline software which is described in next chapter is more important.

3.6 Offline Computing Model

As ATLAS is very complex experiment which might be modified in the future, the software must be robust but flexible enough to follow recent goals of the experiment. ATLAS offline software is based on object-oriented language C++. Some of its components were adopted from other languages FORTRAN or Java. The framework which is used to control the execution flow of the applications like HLT, Simulation, Reconstruction and Analysis is called Athena. It provides the common communication and functionality between different components.

Athena

The Athena framework is an enhanced version of the Gaudi framework originally developed for LHCb experiment. Athena is example of the component-based architecture which very well serves the required flexibility. ESD and AOD are stored in POOL event collection files and are processed using the ATLAS software framework, Athena. Athena is the basic analysis tool. The major Athena terminology

Algorithm in general performs a well-defined and configurable operation on some input data and mostly produces some output data. It implements methods for invocation by framework: initialize(), execute(), begin/endRun() or finalize() [TW]. Algorithm may delegate the processing to AlgTools whose purpose is to help other components perform their work [CTDR].

Job Option files are conventional python scripts (default Job.Option.py) used to control an Athena application configuration at run-time. Via job options the dynamic libraries needed to load are specified and the algorithms are selected. It selects the sequence of the execution and defines the properties of the algorithms [CTDR].

Filters represents the Event selection criteria[TW].

Sequences lists of members Algorithms managed by a Sequencer. Sequencer terminates a sequence when an event fails a filter [TW]. The StopOverride property overrides the default behavior [TW].

ROOT

ROOT is a object-oriented analysis framework which evolved from need of unified set of tools for data analysis of many high-energy physics experiments. It supports various data types frequently used in HEP data analysis like four-vectors and matrix operations. It has various classes for histogramming the data, 3D visualization or fitting measured values. It has it's own C/C++ interpreter CINT which is able to interpret ROOT scripts or even itself. User also has option to compile it in code and dynamically link it as libraries. It has it's own data format for storing ROOT objects, it is used also for storing Atlas data.

4 $Z^0 \rightarrow \mu^+\mu^-$ channel

The $Z \rightarrow \mu\mu$ is important for new physics expected at the LHC and ATLAS in particular. It is also well known decay mode which makes it poverfull tool for calibration of the detector. High-p_T muons are easy to detect and their momentum resolution is good compared to jet energy resolution. It is also relatively clean channel with not much background. In order to account for detector systematics I performed full chain analysis of the $Z^0 \rightarrow \mu^+\mu^-$ channel and found Z-peak in the di-muon invariant mass. The "full chain"simulation refers to the procedure of generation of the Monte Carlo data and letting it pass through detector simulation which models the response of the detector's material and the digitalised signal output which is produced by the detector. Reconstruction is also the part of full chain. I have chosen one of the expected Higgs decay final states $Z \rightarrow \mu^-\mu^+$ which I will pass through the whole simulation process (see Figure 24).

Figure 24: Full chain [TW].

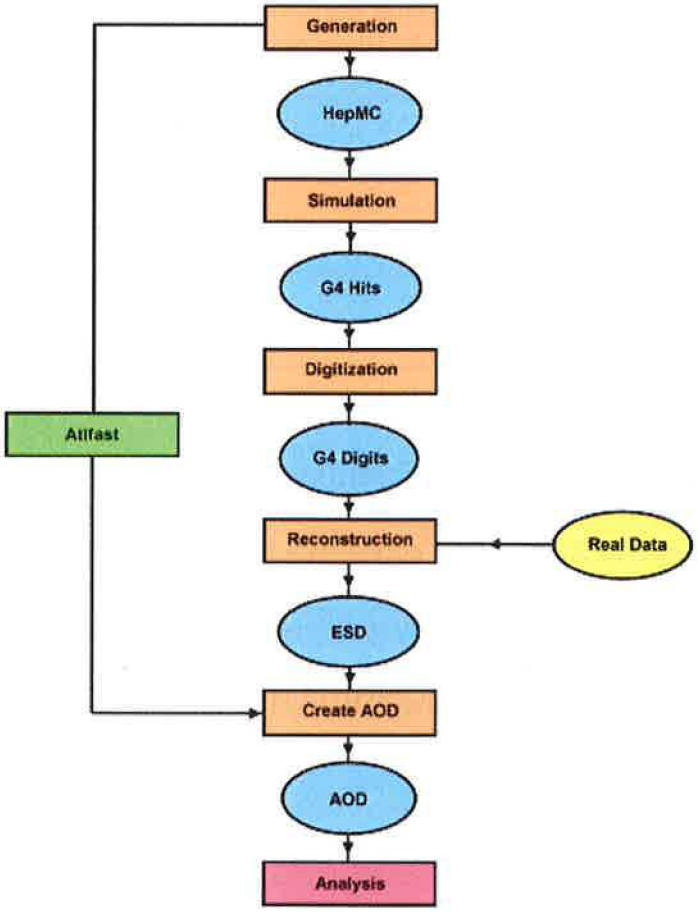

Event Generation is the first stage of the simulation chain, where the software simulates the proton-proton collisions and the subsequent fragmentation, hadronization and all types of decays. A wide range of packages are available for simulating different processes.

One of the widely used generators for the generation of high-energy physics events is called Pythia. It contains theory and models for a number of physics aspects, including hard and soft interactions, parton distributions, initial-state and final-state parton showers, multiple interactions, fragmentation and decay. It is largely based on original research and also on theoretical formulas. Nowadays in ATLAS Pythia is a package for Athena.

In the simulation I performed the center-of-mass energy used for my simulation was 10 TeV. The generator output is a pool.root which is an ATLAS proprietary data format. It contains information and properties of generated particles from Z-$\mu\mu$ channel and event background. I turned off the Multiple interaction which means that I was not considering some of the parton and quark processes because of the channel cleanliness. I used Pythia to generate 100 files, each contained 100 events. Subdividing into multiple files was chosen because of the parallelization of simulation on the Grid. One event represents one pp-collision and creation of one Z boson which consequently decays. In addition to muons there are other collision products as underlying event. Most of this byproducts have significantly low p_T. As you can see in the figure 24 it is possible to swich the Full Chain and go through Atlfast (see figure 24) which provides a fast simulation of the whole chain by taking the generated events and smearing them to produce AOD directly. Atlfast can in fact take input from any of the event generator, simulation, digitization, or ESD files. From the kinematics we get following equation for the Z_0 invariant mass calculated from observables in ATLAS and known muon invariant mass.

$$m_{Z_0}^2 = 2m_\mu^2 + \sqrt{p_{\mu_1}^2 + m_{\mu_1}^2}\sqrt{p_{\mu_2}^2 + m_{\mu_2}^2} - 2\,|p_{\mu_1}|\,|p_{\mu_2}|\cos\alpha \tag{31}$$

The following was computed on LXplus, Cern's public terminal service using Athena release 15.0.0. I have used momentum cut for generated muons which was set at 10 GeV. In order to calculate invariant mass of Z one has to access data inside the root tree. Each branch in event in file(s) is represented as a data vector (i.e. C++ vector of double precision floating point numbers), there are several vectors representing different properties of particles like components of momentum, PDG ID of particle etc. These vectors are bound by a common index used for selection of particles in the event. If abs(PDG)==13 then particle is regarded as muon and invariant mass of first two muons is computed and result is inserted into histogram.

In the figure 25 Z_0-invariant mass peak is clearly visible. Histogram is fitted with Breit-Wigner distribution convoluted with Gaussian distribution.

Breit-Wigner part represents intrinsic distribution of invariant mass from theory and Gaussian part represents smearing due to the errors of measurement. From the fit we see that invariant mass is 91.14 GeV/c^2 which corresponds very well to the experimental value. Sigma (standard deviation) belongs to the Gaussian part (smearing) in the convolution and is small as it is expected for Monte Carlo simulation.

Figure 25: Z_0 invariant mass on the generator level.

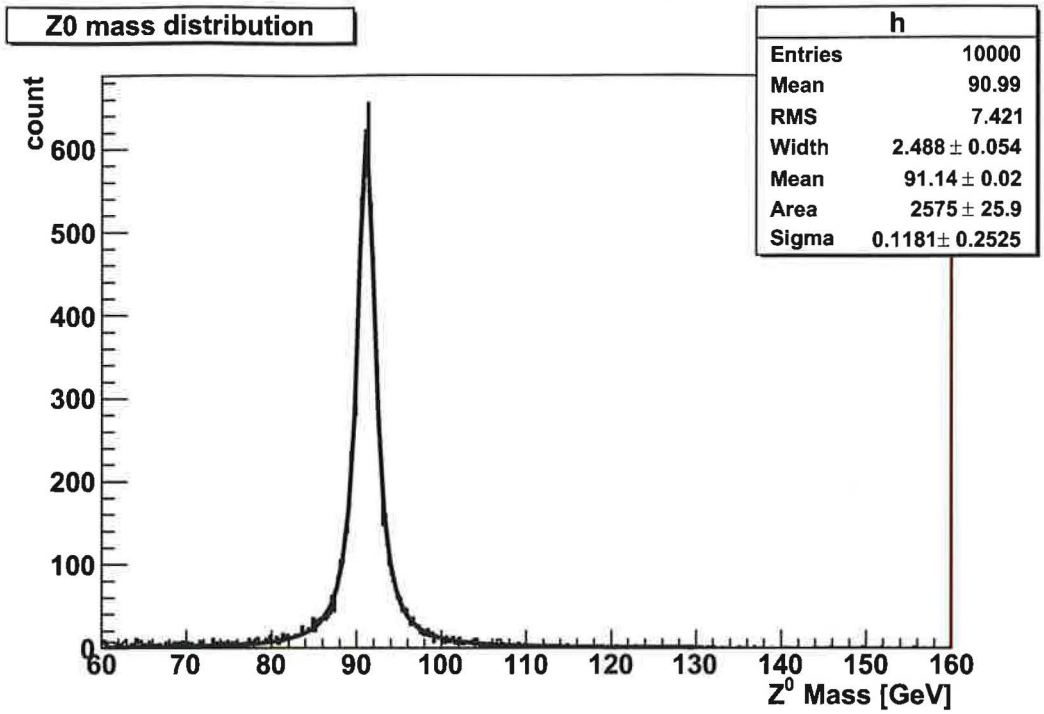

Figure 26: Pythia output, generated muon pseudorapidity.

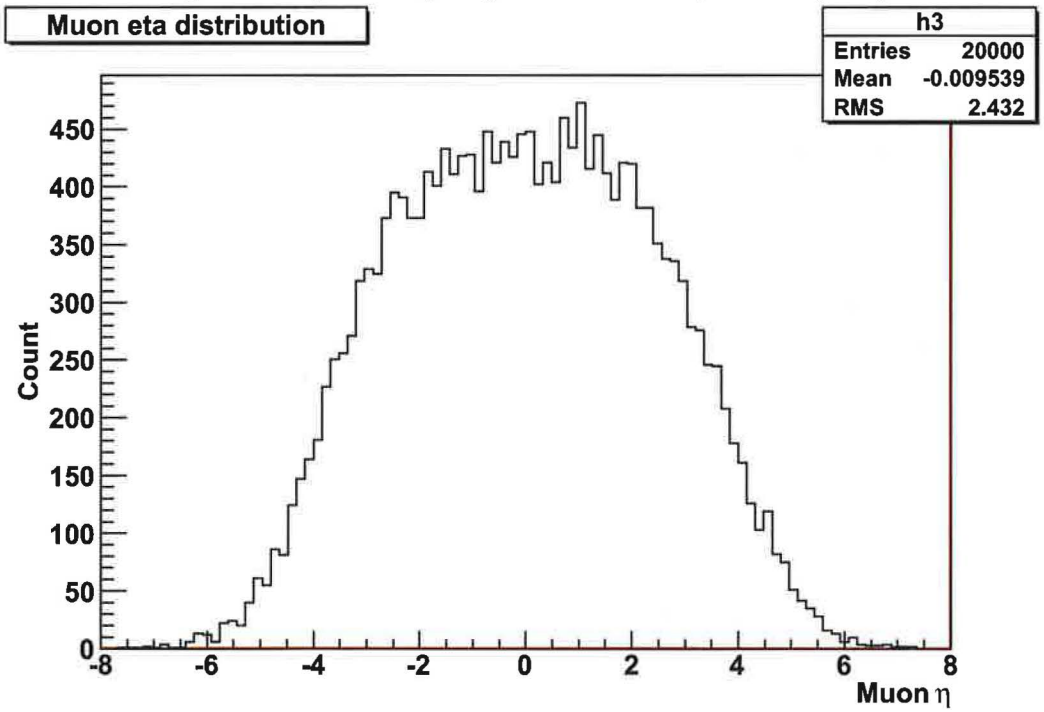

Distribution of pseudorapidity of generated muons on the generator level is shown in figure 26, no cut was made. Events with muons with pseudorapidity -2.5 > η > 2.5 will not be reconstructed in next step because of detector geometry.

Figure 27: Pythia output, trasversal momentum of generated muons.

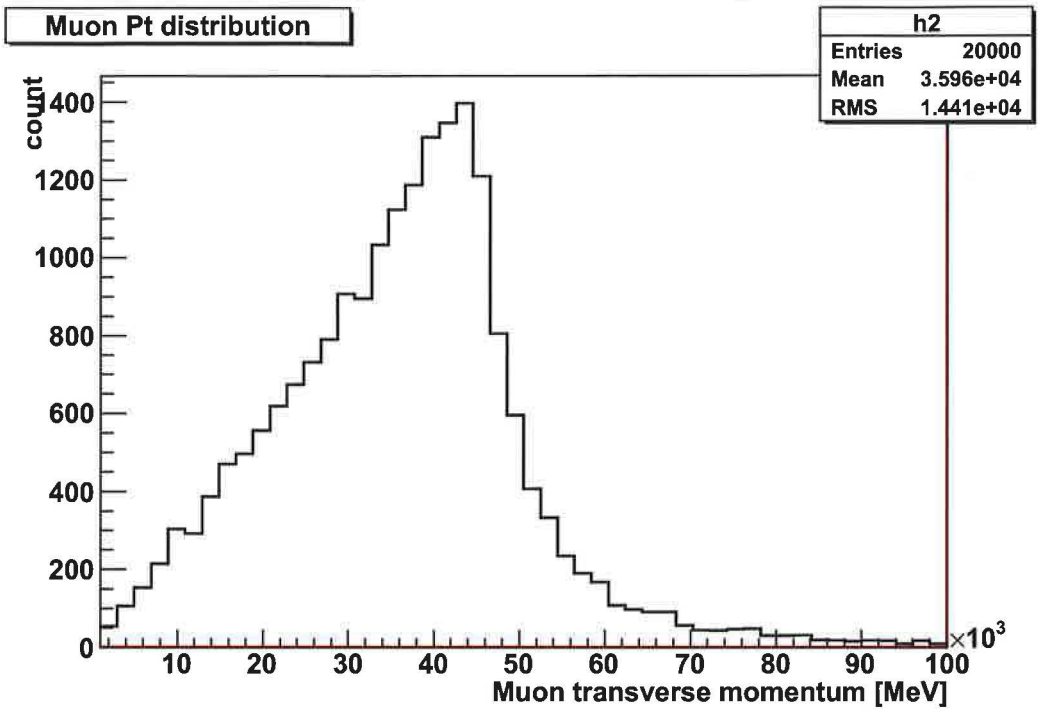

Distribution of transversal momentum of generated muons (figure 27), during generation cut on momentum of 10 GeV was applied.

In the next step I performed simulation on the Grid. Of the one hundred files 85 run through, rest failed for various reasons due to the Grid glitches. It was simulated using Athena transformation script (csc_sim_trf.py) which encapsulates various packages, the most important one being Geant4, which is a framework dedicated for Monte Carlo simulation of passage of particles through material and simulating of the physical response of the detector. Geometrical model of ATLAS I have used is ATLAS-CSC-05-00-00. All the particles from MC simulation in each event are propagated through the detector and each subdetector response (deposited ionization loses) is stored. Digitization, conversion of deposited energy to the digital signal with simulated electronics response is performed also in the simulation script. Output is RDO (Raw Data Object) file. Next step necessary in order to analyse detector response is reconstruction, which is application of various algorithms to the raw data, such as cluster finding, track fitting and particle identification. This was also performed by Athena transformation script (csc_reco_trf.py) using the same geometry tag. AOD was the file type chosen for analysis of dimuons because of it's relatively easy access to data. Since Athena was needed to read AOD.pool.root files, package AnalysisExamples and modified subpackage ZeeZmumuOnAOD was used to find dimuons in the events and plot their properties.

In the histogram on figure 28 invariant mass of Z boson found from the full chain is displayed as well as Breit-Wigner fit with convoluted Gauss distribution. It is visible that even though Z mass is correct, Gaussian part has a large sigma compared to the Z-peak at the generator level which is influenced by the detector effects such as uncertainity of measured muon momentum and misidentification of muons or selecting muon for invariant mass computation which was produced not from Z decay but rather from underlying event.

Out of about 8500 full-chain reconstructed events only 4183 dimuons passed the selection by trigger simulation and charge comparison (muons of opposite charge). Also cut on eta had effect on number of succesful dimuon candidates. Transversal momentum distribution of full chain muons (figure 29) looks similar to the generator-level histogram. Transverse momentum for all found muons is displayed.

In the figure 30 is it shown distribution of pseudorapidity for all reconstructed muons. If one of the muons in dimuon of interest was in the area of pseudorapidity $-2.5 > \eta > 2.5$ detector was not sensitive to it and dimuon was not treated as such.

Figure 28: Z invariant mass from full chain simulation.

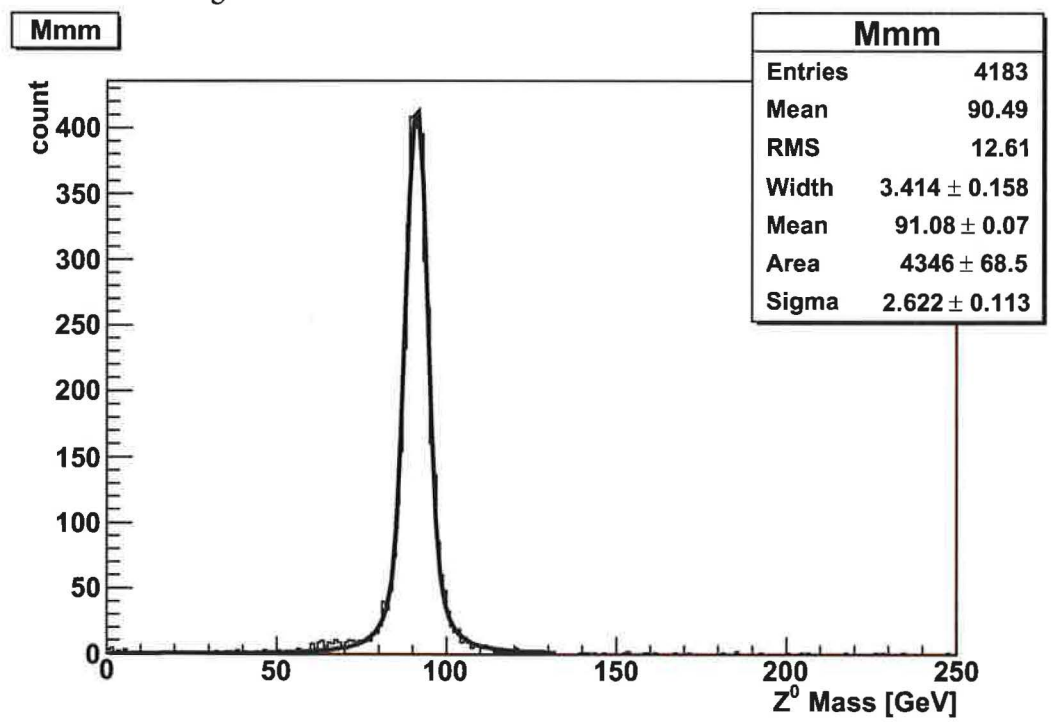

Figure 29: Transversal momentum of particles identified as muons in full chain

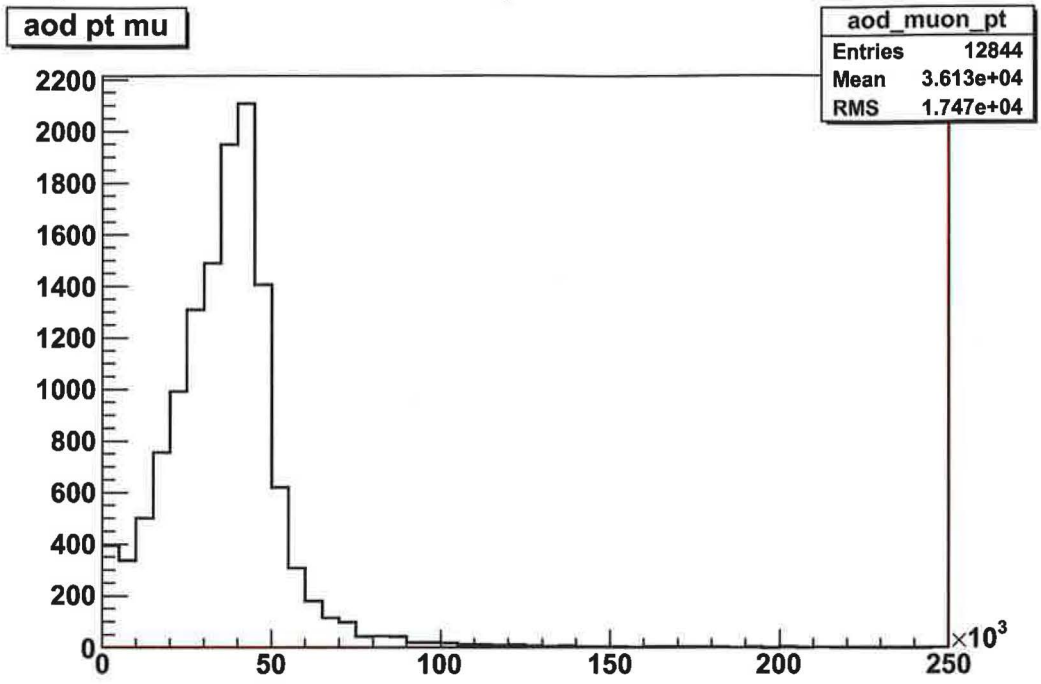

Figure 30: Pseudorapidity of particles identified as muons in full chain.

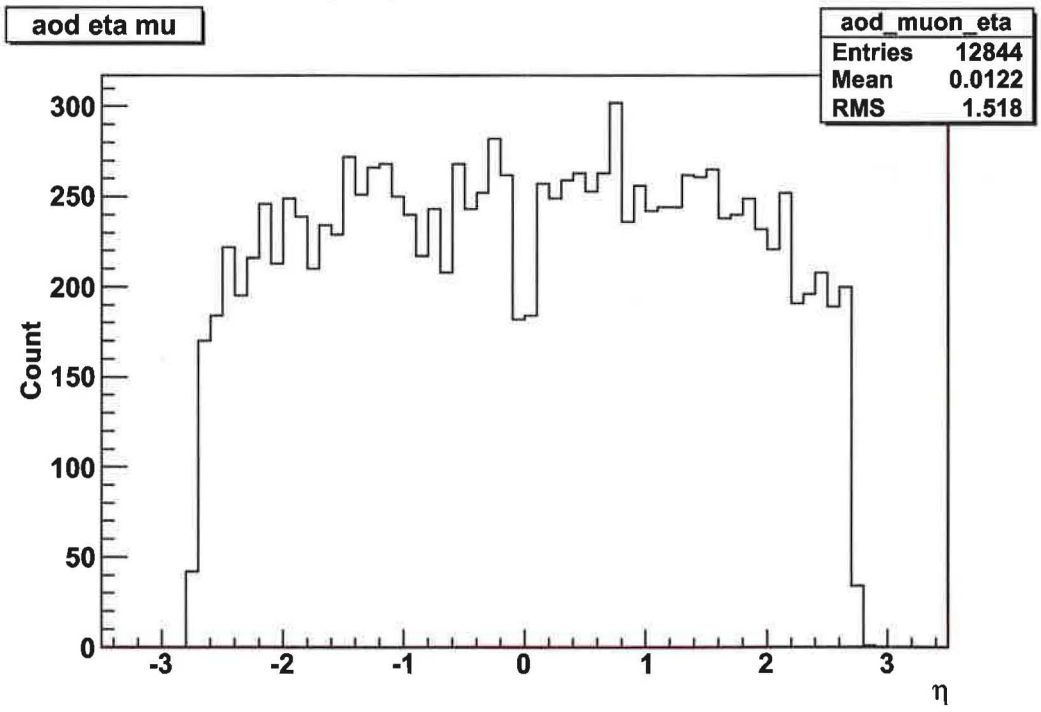

5 Conclusion

I have introduced Standard Model of particle physics and showed some interesting problems of contemporary high-energy physics. I analysed them in relation to existing or planned experiments in the near future, expecially to the ATLAS detector. I made detailed description of the ATLAS and CMS detectors and briefly described dedicated LHC experiments LHCb and ALICE and also TOTEM and LHCf. I briefly introduced two small LHC experiments LHCf and TOTEM. The main parts of this thesis are sections 3 and 4. First one is dedicated to ATLAS data acquisition system and trigger architecture. The other contains analysis of one Z^0 boson decay mode: $Z \rightarrow \mu\mu$ which is very important because of methodical reasons. It demonstates proper functionality of important components of the detectoion system and it also provides a first step to the new physics expected at LHC.

ATLAS detector was completed and commisioned in 2008. LHC is ready for pp-collisions in late 2009 it will be able to take a look at new physics hiding behind the energy frontier.

List of publications

[ALD] *Aldebaran Group for Astrophysics [online]*: **www.aldebaran.cz [cite 23/4/2009].** Last update 23/4/2009.

[ALDR] *ALICE Collaboration (2001)*: **ALICE Technical Design Report.** CERN Geneva, CERN-LHCC-2006-014.

[ALDS] *Gustafsson H. Å. for The ALICE Collaboration (2007)*: **ALICE Detector Status and Commissioning.** CERN Geneva and Lund University Sweden

[ALMS] *Espagnon B. for The ALICE Collaboration (2008)*: **The ALICE muon spectrometer and related physics.** Journal of Physics G: Nuclear and Particle Physics, IOP Publishing Ltd, UK.

[ALpo] *ALICE Collaboration (2002)*: **ALICE Time Projection Chamber Poster.** CERN Geneva.

[ARPC] *Instituto Nazionale di Fisica Nucleare [online]*: **http://sine.ni.com/cs/app/doc/p/id/cs-10283 [cite 18/4/2009].** Last update [18/4/2009].

[ATDR] *The LHCb Collaboration (2003)*: **LHCb Addendum to the Muon System Technical Design Report** CERN Geneva.

[CMS] *The CMS Collaboration (2006)*: **CMS Physics Technical Design Report Volume I: Detector Performance and Software.** CERN Geneva

[CRO] *Bederson B., Walther H. (1994)*: **Advances in Atomic, Molecular and Optical Physics Vol. 33** Academic Press UK, ISBN-13: 978-0120038343.

[CTDR] **The ATLAS Computing Group (2005)**: ATLAS Computing Technical Design Report. CERN Geneva, CERN-LHCC-2005-022, ISBN: 92-9083-250-9.

[EMB] *Aharrouche M., Colas J. et al. (2008)*: **Energy Linearity and Resolution of ATLAS Electromagnetic Barrel Calorimeter in a Electron Test-Beam.** CERN Geneva.

[EMEC] *The ATLAS Electromagnetic Liquid Argon Calorimeter Group (2002)*: **Performance of the ATLAS Electromagnetic Calorimeter End-Cap Module 0.** CERN Geneva.

[EW] *Quigg Ch. et al. (2009)*: **Unanswered Questions in the Electroweak Theory**, Cornell University Library ArXive e-print service, arXiv:0905.3187

[FR] *Jakobs K. (2009)*: **Physics at Hadron Colliders.** Lecture given at XIV. LNF Bruno Touschek Spring School; Frascati Italy.

[Gr1] *Heinemeyer S. [online]*: **<http://dorigo.wordpress.com/> [cite 24/5/2009].** Last update 24/5/2009.

[Gr2] *Tevatron New Phenomena and Higgs Working Group [online]*: **<http://tevnphwg.fnal.gov/results/SM_Higgs_Fall_07/tevlog_nogrid.eps> [cite 24/5/2009]**, last update 14/12/2007

[Gr3] *CERN - media archive [online]*: **<http://mediaarchive.cern.ch> [cite 24/5/2009]**. Last update 20/5/2009.

[LAr] *Dannheim D. on behalf of the ATLAS Liquid Argon Calorimeter Group (2008)*: **Commissioning and Performance of the ATLAS Liquid Argon Calorimeters.** CERN Geneva.

[LHCf] *The LHCf experiment at LHC [online]*: **http://www.particle.cz/conferences/c2cr2005/talks/Adriani.pdf [11/5/2009]**. Last update 9/9/2005.

[LHCf2] *LHCf experiment homepage [online]*: **http://hep.fi.infn.it/LHCf/Pages/ExperimentPage.html [cite 11/5/2009]**. Last update 11/5/2009.

[Mag] *Miele P., Cantaneo F., et al. (2004)*: **ATLAS Magnet Common Cryogenic, Vacuum, Electrical and Control Systems.** IEEE Explore Digital Library, Transactions on applied superconductivity vol. 14 issue 2

[MDT] *Brandenburg G. (2007)*: **ATLAS Monitored Drift Tube Readout Electronics.** Talk Given at Harvard Group Meeting

[Mol] *Swanson W. P. and Thomas R. H. (1990)*: **Dosimetry for Radiological Protection at High-Energy Particle Accelerators.** New York, Academic Press.

[MTDR] *The LHCb Collaboration (2001)*: **LHCb Muon System Technical Design Report.** CERN Geneva.

[Muon] *Vlachos S. on behalf of the ATLAS collaboration (2009)*: **Status and performance of the ATLAS MUON spectrometer.** NIMS, Athens, ATL-MUON-PROC-2009-002.

[Oxf] *Oxford LHCb and CLEO-c* : **http://www-pnp.physics.ox.ac.uk/~lhcb/rich.shtml [cite 20/4/2009]**. Last update 18/4/2009.

[Pc1] *University of Toronto particle physics homepage [online]*: **http://hep.physics.utoronto.ca [25/5/2009]**. Last update 30/10/2008

[Pix] *G. Aad, M. Ackers et al. (2008)*: **ATLAS pixel detector electronics and sensors.** IOP Publishing Ltd and SISSA.

[RICH] *The LHCb Collaboration (2000)*: **LHCb RICH Technical Design Report.** CERN Geneva.

[RICH2] *Members of the LHCb RICH group (2002)*: **LHCb RICH 2 Engineering Design Review Report.** LHCb EDR 2002-009, CERN Geneva.

[RPC] *Pietra M. D. (2005)*: **Performance test and quality, assurance of RPC trigger chambers for ATLAS experiment and LHC.** INFN, Napoli, Italy.

[SM] *Cottingham W. N., Greenwood D. A. (2007)*: **An Introduction to the Standard Model of the Particle physics Second Edition.** Cambridge University Press, UK.

[TiCa] *Leitner R. for the ATLAS Collaboration (3/6/2002)*: **Status of the ATLAS Hadronic Calorimeter.** Talk given at the 3rd International Workshop on Very High Multiplicity Physics, Dubna.

[TOT] *Deile M. et al. (2006)*: **Diffraction and Total Cross-Section at the Tevatron and the LHC.** Cornell University Library ArXive e-print service, arXiv:hep-ex/0602021v1.

[TPC] *ALICE Collaboration homepage [online]*: **http://aliceinfo.cern.ch/Public/en/Chapter2/Chap2_TPC.html [cite 10/5/2009].** Last update 13/2/2009.

[TS] *van Hunen J. J. et al. (2006)*: **The LHCb tracking system.** École Polytechnique Fédérale de Lausanne

[TW] *The ATLAS Twiki [online]*: **<https://twiki.cern.ch/twiki/bin/view/Atlas/WebHome> [cite 25.5.2009].** Last update 20/4/2009.

[Wi] *Wikipedia the free encyclopedia [online]*: **http://en.wikipedia.org/ [cite 15/3/2008].** Last update 15/3/2008.